Light-driven modulation of liquid-crystalline order in the nematic phase with azobenzene-containing copolymer

Chien, Chiao-Ying

2020

Table of Contents

Abstract

Manipulation of impurities in liquid crystal (LC) has received wide interests since it helps develop tunable functional composites, such as photonic elements, molecular motors, and biological sensors. It has been reported that flexible polymer could be transported through spatial variation of the scalar order parameter (*S*) in the nematic LC. The spatial variation of *S* in this molecular manipulator was generated by stimulating the *trans*-to-*cis* isomerization of azobenzene derivatives in the nematic phase. Under UV light, the trans-azobenzene converts into *cis* form. The *cis*-azobenzene with a bent-like shape tends to destabilize the liquid-crystalline order, resulting in a decrease of *S* and the birefringence (Δn) of the nematic phase. Based on this mechanism, the molecular manipulator has a great potential to drive arbitrary nanometer-sized impurities in the nematic phase. However, this method has a limitation. The natural diffusion of azobenzene might cause poor spatial resolution of *S*, which obstructs the development of precisely-controlling the nm-sized impurities.

This thesis aims to solve the current limitation of the molecular manipulator. Herein, immobilization of azobenzene through polymerization is proposed to prevent the diffusion of azobenzene in the nematic phase. Azobenzene-containing monomer is *in-situ* polymerized with diacrylate monomer in the nematic phase, resulting in the formation of LC gels with the phase-separation of azobenzene-containing copolymer microstructure. In chapter 2, a newly observed photo-response of LC gels is reported. Unlike typical photo-induced decrease of Δn in the azobenzene/nematic mixture, an increase of Δn is observed under UV irradiation in the LC gels. To clarify the origin of this abnormal photo-response, the photo-induced change of Δn and the morphology of the copolymer microstructure are investigated with the variant composition of LC gels. The mechanism of abnormal increase of Δn is considered as follows. The shape of the copolymer microstructure, which have a finite anchoring strength on their

surface, influence the LC director and result in a lower Δn before the UV irradiation. The *trans*-to-*cis* isomerization of azobenzene weakens the surface anchoring of the copolymer microstructure. Hence, the LC directors recover their uniform distribution, and the increase of Δn appears.

In chapter 3, the resolution of photo-induced spatial variation of S in the LC gels is studied. To simplify the experiment, the composition of LC gels is tuned to eliminate the abnormal increase of Δn and evaluate the spatial resolution of the LC gels. The photo-induced spatial variation of Δn of the non-polymerized and the polymerized samples are quantitatively compared through measuring their full-width-at-half-maximum (FWHM). The FWHM of the non-polymerized sample expands with time, while the polymerized sample remains the feature close to that of the stimulating light. The time evolution of Δn clearly shows that the photo-induced change of S is highly constrained in the irradiated area in the polymerized sample. Based on these results, the LC material for modulating the scalar order parameter with a high spatial resolution has been successfully achieved in this thesis.

Publications:

(1) Chiao-Ying Chien and Jun Yamamoto, “Photo-induced recovery of liquid crystalline order with azobenzene-containing copolymer in nematic liquid crystal", submitted.

(2) Chiao-Ying Chien and Jun Yamamoto, “Light-driven modulation of scalar order parameter for high spatial resolution” *Europhysics letters*, 131, 26001 (2020).

Chapter 1 Introduction

Liquid crystals (LCs) are mesophases between solid (crystalline) and liquid (isotropic) states. It has some properties of the liquid (such as fluidity), as well as crystalline properties (optical, electrical, elastic properties, etc.)[1]. Due to their unique properties, scientists can make them be suitable materials for many other applications in broad fields. Manipulation of impurities in LCs has sparked a surge of interest in these two decades[2–9]. Many fascinating phenomena were reported with dispersing various impurities, such as colloids, noble metal particles, and polymer, into the LC medium. The behavior of these impurities in the LC medium is strongly related to the size of impurities[8,9]. The micrometer-sized impurities, such as colloids and water droplets with a large diameter, could distort the surrounding LC director field through the anchoring at their surface. Manipulating the μm-sized impurities through the elastic distortions of the LC director field has been well-explored and understood, leading to the development of novel nematic colloidal crystals[10,11].

On the other hand, the impurities in nanoscale, *e.g.* molecules or polymer, retain the uniform LC director field around them since the anchoring energy was much weaker than the elastic energy of distortion[8,9,12]. Therefore, the transportation driven by the elastic distortion energy of LC was no longer capable in nanoscale. A recently reported method described the transportation of nanometer-sized impurities through the photo-induced spatial variation of liquid-crystalline order[12]. Such a method could manipulate arbitrary nm-sized impurities in the nematic phase since the transportation is simply guided along with the spatial variation of the scalar order parameter (S) instead of the LC director field. However, because the spatial variation of S was generated through the implanted azobenzene in LC, the natural diffusion of azobenzene molecules might cause poor spatial resolution of S, which hinders the precision of the manipulated impurities[13–15].

In this chapter, we first give an introduction of nematic LC and then discuss the current technics of manipulation in the nematic phase. The mechanism of photo-stimulated spatial variation of *S* in the nematic LC through isomerization of azobenzene is also described in detail. Finally, to manipulate the impurities of nanoscale in the nematic phase with high precision, we propose a method to solve the current limitation of the molecular manipulator.

1.1. **Nematic phase**

Liquid crystals are characterized by different mesophases, which depend on their arrangement: the degree of orientation and order of position. The nematic phase is characterized by only orientational order, in other words, no order of position. The long axes of the molecules tend to be parallel to a direction, yielding a uniaxial nature of the nematic phase (**Fig. 1.1**). The preferred orientation of LC molecules is defined by a unit vector **n**, which is called director[1,16–18], as noted in **Fig.1.1**. There is no distinction between director **n** and **-n**.

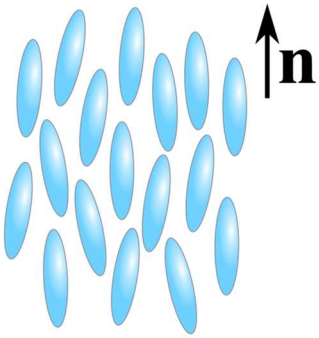

Fig. 1.1 Schematic image of the nematic phase with rod-like LC molecules. The unit vector **n** describes the local preferred direction of the LC molecules.

The degree of the orientational order of the nematic phase can be statistically quantified by the scalar order parameter *S*[16]:

$$S = \frac{1}{2}\langle 3\cos^2\theta - 1\rangle = 2\pi \int_0^{\pi} P_2(\cos\theta) f(\theta) \sin\theta d\theta, \quad (1)$$

where θ is the angle between an axis and the director **n**, $f(\theta)$ represents the distribution function of the director **n**, $\langle \ldots \rangle$ is an average overall molecular orientation, and $P_2(\cos\theta) = \frac{1}{2}(3\cos^2\theta - 1)$ is the Legendre polynomial of the second order. By this means, $S = 1$ for the most ordered state, and $S = 0$ for the isotropic state since all orientations in space have equal probabilities (**Fig. 1.2**). Noted that the real values of the scalar order parameter of the nematic phase are smaller than 1 due to the thermal fluctuations[16]. The scalar order parameter is temperature-dependent (**Fig. 1.3**). By increasing the temperature (T), the nematic phase undergoes first-order N-I transition at T_c, where T_c is the phase-transition temperature of the nematic to isotropic phase, and then the scalar order parameter vanishes in the isotropic phase[16].

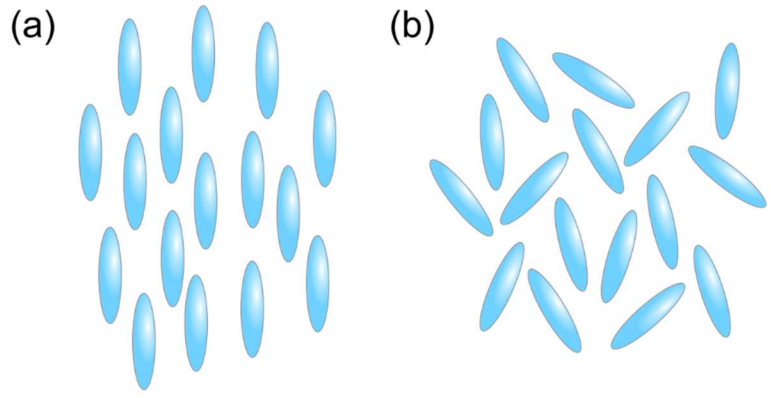

Fig. 1.2 Schematic image of (a) the most ordered state and (b) the isotropic state.

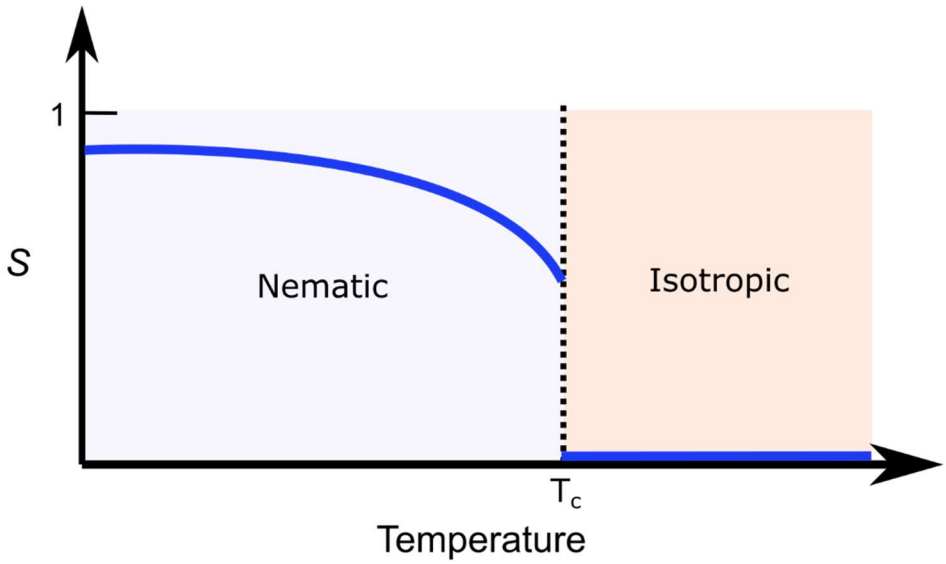

Fig. 1.3 The scalar order parameter as a function of temperature.

Since the nematic phase is the simplest mesophase, it has received wide attention and has been utilized in various fields, such as photonics and manipulation. In the next section, we give an overview of the manipulation in the nematic phase. The photonic LC materials based on azobenzene derivatives will be introduced in section 1.3.

1.2. **Manipulation in nematic**

In this section, we introduce the manipulation of impurities in the nematic phase with two categories: macro-sized impurities and nano-sized impurities.

1.2.1. Macro-sized impurities

Behaviors of micrometer-sized impurities, such as colloids, in the liquid crystals (LC), is greatly dependent on the elastic distortion of the LC director field[2–9]. The theoretical study was first developed by Lubensky *et al*. to explain the behavior of particles in the nematic host[19]. Suppose a particle with a radius of R, which prefers a perpendicular anchoring on the surface, is placed into a uniform nematic phase. The presence of the micro-sized particle in an LC phase tends to distort the original uniform LC director field, resulting in an elastic distortion[9]. The elastic energy of the distortions is approximately linear with R: $F_{\text{elastic}} \sim KR$, where K is the elastic constant of LC[8]. On the other hand, the surface anchoring of the particle dominates the surrounding LC director, yielding the anchoring energy that scales to the surface area, $F_{\text{anchoring}} \sim WR^2$, where W is the surface anchoring coefficient[8]. The values of W have a wide range of $10^{-6} \sim 10^{-3}$ J/m^2, depending on the material of the surface[20]. The ratio of the elastic constant to the surface anchoring coefficient has the dimension of length $a = K/W$, which is known as surface extrapolation length, or de Gennes-Kleman length[21]. The LC director fields of the particle-implanted nematic phase are related to the balance between the two energies: KR and WR^2. For the large particle with the size of $R \gg K/W$, the LC director field is strongly distorted to satisfy the anchoring condition on the surface of the particle (**Fig. 1.4a**). When the size of the particle is small enough to fulfill $R \ll K/W$, the anchoring effect becomes relatively weak, resulting in a uniform LC director field surrounds the particle (**Fig. 1.4b**)[8,9,12].

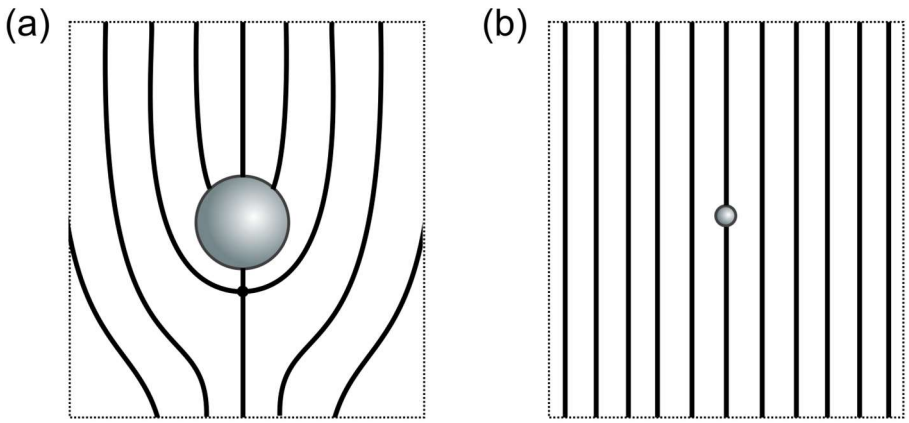

Fig. 1.4 The director fields surrounding spherical particles: (a) the dipolar structure with a hyperbolic hedgehog defect induced by large particle, and (b) the uniform director field with small particle.

The distortion of director fields could lead to anisotropic interactions between the spherical particles in the nematic phase[5,6,9]. When two spherical particles are placed close to each other, the distortion around them starts to overlap, suggesting that the total energy of the pair of particles is dependents on the particle separation[22]. The director fields distorted of the two particles result in the anisotropic interparticle forces with values of pN order[5]. This anisotropic interactions mediated by the elastic distortion could overcome Brownian motion when the distance between the two particles is less than 3 particle diameter[6]. The distortions of the director fields induced by large spherical particles usually have the dipolar or quadrupolar symmetry[7,23]. In the case of distortion is dipolar symmetry (see an example in **Fig 1.4a**), the interparticle forces could lead to the formation of 1D chain[2,5–7,9,24], or 2D arrays with the assistant of optical tweezer[25–27].

1.2.2. Nano-sized impurities

As we already discussed in 1.2.1, it is difficult to manipulate the nanometer-sized impurities through the elastic distortion of the LC director field because of its large energetic cost. Entropic forces become important in the manipulation of nm-sized impurities[8,9]. Samitsu *et al*. first proposed that the spatial variation of the scalar order parameter (*S*) could drive the manipulation on the molecular level[12]. Such spatial variation of *S* was performed by stimulating the implanted azobenzene derivatives in the nematic phase with UV light [28–30]. They demonstrated that photo-induced spatial variation of *S* could guide the transportation of fluorescent polymer. The presence of flexible polymer didn't induce distortion of the LC director field but disturbed the liquid-crystalline order and increased the free energy of the system[12,31]. Based on this, Samitsu *et al*. predicted a direct coupling between *S* and the concentration of polymer. In their study, the fluorescent polymer was found to accumulate to the irradiated area after the spatial variation of *S* was induced through the UV irradiation, resulting in an increase of fluorescence intensity within a region of ~ 200 μm (**Fig. 1.5**). The change in the concentration of manipulated impurities was proportional to the change in *S*, which was represented intern of decrease of birefringence. By this means, the polymer could be controlled to accumulate to any position in the nematic phase by UV light.

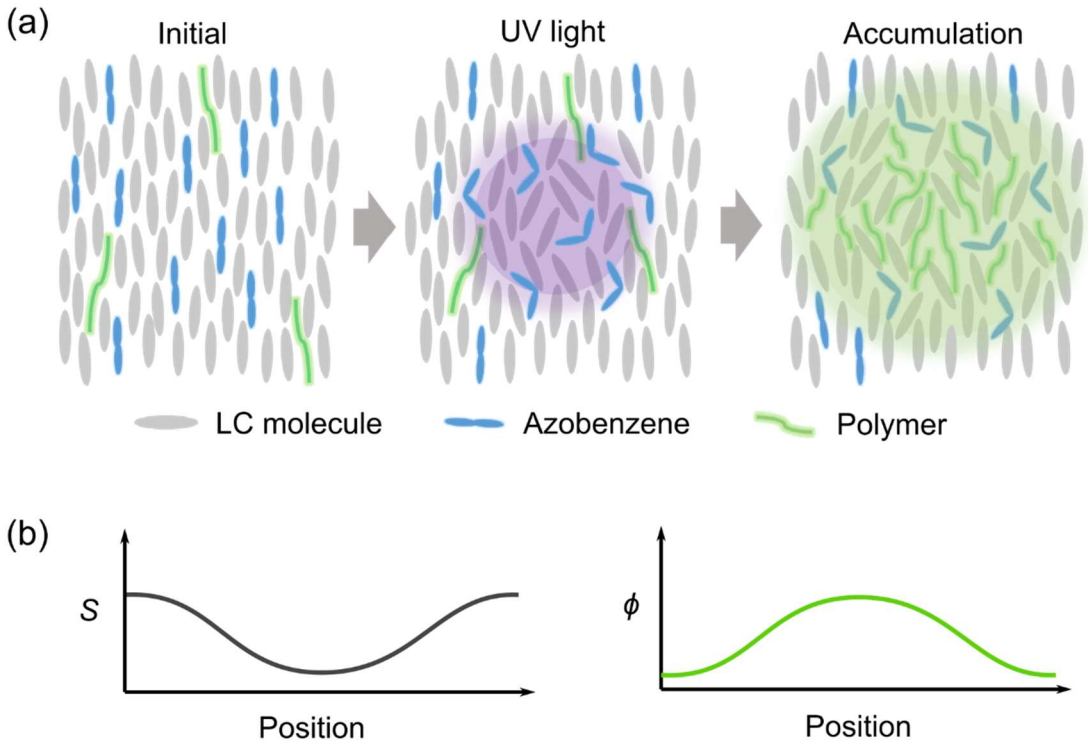

Fig. 1.5 (a) The schematic illustration of the molecular manipulator. (b) The spatial variation of the scalar order parameter (S) induced by the isomerization of azobenzene in the nematic phase, and the resulting distribution of the fluorescence polymer concentration (ϕ).

Similar to the work of Samitsu *et al.*, Škarabo and co-workers recently demonstrated that the spatial variation of the scalar order parameter induced by heating the local nematic phase could also transport fluorescent molecules[32]. They used a laser beam to focus on the ITO layers of the planar LC cells. Absorption of laser light in the ITO layers caused the increase of temperature at the local nematic phase, resulting in a decrease of S in a relatively large area (~ 100 μm). A prior study of transporting charged μm-sized colloidal particles through the thermally-induced spatial variation of S had been already reported by another group[33], in which they provided a possible explanation that the motion was attributed to the flexoelectric effect induced by the radial distribution of the S. In the report of Škarabo *et al.*,

they also studied the transportation of μm-sized colloidal particles and fluorescent dyes by using the thermally-induced spatial variation of *S*. Based on the evidence that the trapping potential scaled linearly with particle radius, they proposed that the trapping mechanism of μm-sized particles attracted into the heating area is attributed to the elastic energy of the distorted LC around the particle and the softening of the elasticity of LC with the increased temperature. They demonstrated that this thermally induced spatial variation of *S* could drive the nm-sized fluorescent molecules as well, though it was still questionable that whether the trapping mechanism is the same as that of the μm -sized particles.

Other researchers have devoted to studying the interaction of nanoparticles (tens to hundreds of nm) in the nematic phase and reported that the anchoring condition of the nanoparticles is an important factor in this system[9,22,34,35]. Koenig Jr. *et al*. observed the long-range interparticle attraction with gold nanoparticles of diameter 170 nm, which had a weak homeotropic anchoring in LC[34]. This attraction was not observed in the case of the gold nanoparticles with planar anchoring. On the other hand, Ryzhkova *et al*. studied the attraction between the pair DMOAP-treated silica nanoparticles, which had a very strong homeotropic anchoring strength in LC. They found that the nanoparticles could form a stable pair with a size of 35 nm diameter[35]. On the contrary, for the nanoparticles with a diameter of 22 nm, they found that the elastic interaction force is almost equal to Brownian force, and thus it couldn't form stable pairs. There also have several groups focused on manipulating nanoparticles through the gradient of the director field and topological defects[8,9,36]. Voloschenko *et al*. reported that during the photo-stimulated polymerization, the phase-separated particle (photopolymer) migrated to the location where the director was strongly distorted, and thus reduced the total energy of the system[37]. According to this, it can expect that the nanoparticles would still be attracted to the LC defects to reduce the energetic cost of the distorted regions[8,9]. Senyuk *et al*. demonstrated that the nanoparticles with different

shapes could transport into the point defect that induced byμm-sized particles in the nematic phase[36]. The studies of the interaction between nanoparticles and topological defects were widely investigated in the blue phase, which has a double twisted structure with periodic defects[9,38,39].

To conclude, the manipulation of nanometer-sized impurities in the nematic phase is still a challenging issue. It needs to put extra efforts, such as implanting azobenzene derivatives into LC, modifying surface anchoring of the nanoparticles, or heating the LC, to achieve suitable conditions for manipulating in the nematic template. The molecular manipulator proposed by Samitsu *et al*. has a great potential to manipulate arbitrary functional impurities in the nematic phase. The impurities can move along with the spatial variation of *S*, which is generated by the photo-stimulating isomerization of azobenzene in the nematic phase. In the next section, we described the mechanism of the photo-induced decrease of *S* through the azobenzene derivatives in the LC phase in detail.

1.3. **Photo-controllable LC with azobenzene derivatives**

Isomerization of azobenzene could be utilized to achieve photo-responsive liquid crystals[28,29,40,41]. Such as inserting molecular containing azobenzene-group into the LCs or modifying the alignment layer with azobenzene derivatives of LCs, numbers of LC functional applications have been developed with the unique photo-stimulated reaction of azobenzene. In this section, we first introduce the photoisomerization of azobenzene and then overview the current applications based on the azobenzene/nematic system.

1.3.1. Isomerization of azobenzene

Azobenzene derivatives are compounds that consist of two phenyl rings with a bridge of N=N double bond. Isomerization of azobenzene occurs under light irradiation in a certain spectral range. As shown in **Fig. 1.6**, a *trans*-azobenzene converts to a *cis* form under UV illumination (λ = 300 nm ~ 400 nm), and reverses to the *trans* form via thermal relaxation or visible light illumination (λ > 400 nm)[29,42]. The isomerization in azobenzene can take place along two different pathways in the nπ^* and $\pi\pi^*$ states[42–44]. The trans-azobenzene has a strong $\pi\pi^*$ band (electronic excitations of the π-conjugated system) and a very weak nπ^* band (electronic excitations of the azo linkage). In contrast, the $\pi\pi^*$ band of the *cis*-isomer is weak but its nπ^* band is stronger than that of the *trans* form. Accordingly, irradiation in UV spectral range allows π-π^* transition, predominantly the *trans*-azobenzene isomerizes into the *cis*-azobenzene. Similarly, irradiation of blue light which corresponds to n-π^* transition can induce the *cis*-to-*trans* isomerization. The absorption band of the azobenzene can be modified to shift to the visible light region through the ring substitution pattern[29], thus, there has a wide various type of azo dyes. The *trans* isomer is thermodynamically more stable than the *cis* isomer[41]. The *cis* isomer spontaneously

thermally converts back to *trans* isomer in the dark, with a time scale ranging from seconds to hours, depending on the substitution pattern of azo dyes and the local environment[29].

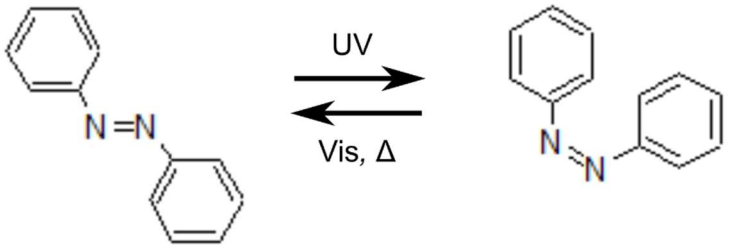

Fig. 1.6 Schematic image of the azobenzene photoisomerization.

The azobenzene shows another interesting behavior under irradiation of linear polarized light. Since the *trans* azobenzene has π-π* transition nearly parallel to the long molecular axis, the probability of absorption of the linearly polarized light is dependent on the angle between the transition dipole axis and the light[29,45]. Assume the *trans* azo dyes initially have an angular distribution (**Fig. 1.7**). Under the irradiation of linearly polarized light, the *trans* isomers isomerize to the *cis* form and then reconvert into *trans* form with a new direction. The *trans*-to-*cis* isomerization is inactive only when the *trans* azobenzene reorients to the direction perpendicular to the polarization direction of light. Consequently, all azo dyes align to the direction perpendicular to the linearly polarized light and give rise to the birefringence.

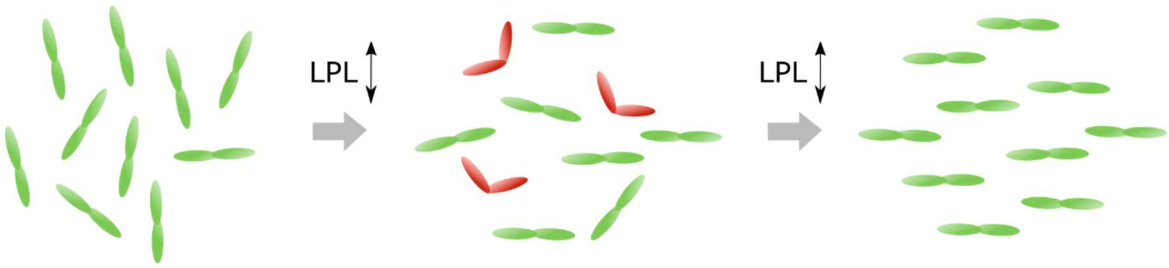

Fig. 1.7 Reorientation of azobenzene under linearly polarized light (LPL).

1.3.2. Photo-responses in azobenzene-containing nematic LC systems

Dispersing a small amount of azobenzene derivative into the nematic phase results in a guest/host system that can respond to light[40]. Since the LCs react sensitively under external stimuli, a change in the orientation of a small portion of the LC molecules stimulated by guest molecules could lead to a change of the orientation in the whole system[40]. In the azobenzene/nematic LC system, the *trans*-to-*cis* isomerization tends to destabilize the liquid-crystalline order[30,40]. The *cis* isomers having a bent-like shape disturb the liquid-crystalline order of the rod-like LC molecules. The optical birefringence ($\Delta n = n_{\parallel} - n_{\perp}$) of nematic LC, which is related to the scalar order parameter of liquid crystal (S), is decreased by the *trans*-to-*cis* isomerization of azobenzene. If the temperature of the azobenzene/nematic mixture with *trans* from is set to near the nematic-isotropic transition temperature (T_c), the photo-stimulated *trans*-to-*cis* isomerization would lower T_c, and induced the photochemical phase transition (**Fig. 1.8**)[40,45]. It was reported that the photochemical phase transition was greatly dependent on the shape of the *cis* isomers[46]. For the *cis* isomers and the *trans* isomers both have similar rod-like molecular structures, no

photochemical phase change of the nematic phase can be observed even doped with 20 wt%[46]. The interaction between the guest molecules and the host nematic phase was also important in the photochemical phase transition. Iketa *et al*. reported that an odd-even effect of the alkyl spacers was observed on the orientational ordering of the mesogenic azobenzene derivatives in the nematic host[47–49]. The azobenzene guests which had higher orientational ordering in the nematic host caused the photochemical phase transition more effective.

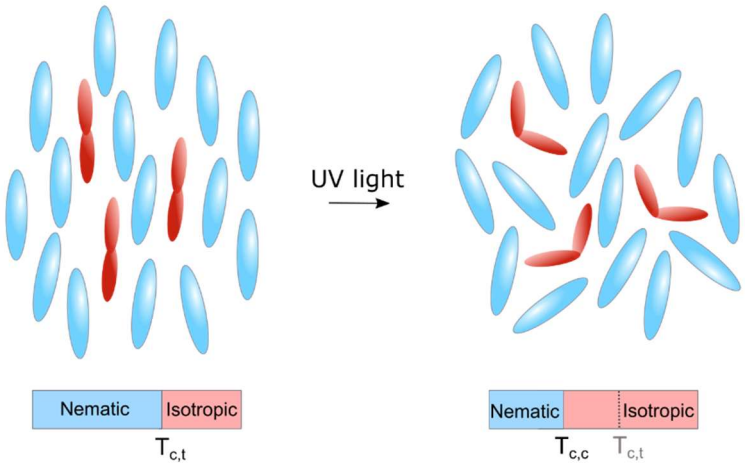

Fig. 1.8 The nematic-to-isotropic transition temperature of the azobenzene-doped nematic phase with *trans* isomers and cis isomers, which is defined as $T_{c,t,}$ and $T_{c,c}$, respectively. The molecules colored by red represent the azobenzene derivatives while the molecules colored by blue represent the LC molecules.

The photoresponses of azobenzene-containing nematic LC systems and their functional photonic applications have been received wide interest since the 1990s. It can be divided into several types. As we have introduced in the previous paragraph, the low-molecular-weight azobenzene derivatives dissolved in the low-molecular-weight nematic phase, *e.g.* 5CB and 7CB, is the most basic type in the azobenzene/nematic LC systems. The previously

mentioned molecular manipulator is the first example of manipulating impurities though the spatial variation of the scalar order parameter via the isomerization of low-molecular-weight azobenzene[12]. On the other hand, the polymer liquid crystals (PLCs) have been utilized to perform optical image storage systems through the photochemical phase transition. Ikeda *et al.* first demonstrated the photochemical phase transition in PLCs by doping low-molecular-weight mesogen with azobenzene group in the PLC film[50–52]. Since the low-molecular-weight azobenzene derivatives were usually hardly-soluble in PLCs, polymers which contain azobenzene moieties and show a nematic phase are later to be regarded as another promising photonic LC material for developing optical image storage systems[45]. The photochemical phase transition of the azobenzene-containing liquid-crystalline polymers is very essential compared to the usual low-molecular-weight guest/host systems. Eich *et al.* first demonstrated a hologram with the use of liquid-crystalline polyester containing mesogenic groups of the azobenzene type in the side chain[53]. Ikeda *et al.* developed azobenzene liquid-crystalline polymer films that could rapidly respond to light with the time scale of microseconds[54].

The azobenzene-containing nematic systems based on the photochemical phase transition have been studied for the novel applications *e.g.* optical switching devices and optical memory storages, at the same time, several groups studied the photo-controlling alignment of azobenzene liquid-crystalline polymer films through the reorientation of azobenzene[55–58]. Since the isomerization of azobenzene is inactivated when the azobenzene dipole axis is perpendicular to the polarization direction of light, the irradiation of linearly polarized light results in the generation of optical anisotropy in the azobenzene-containing polymer LC material[56,59]. The azobenzene-containing alignment layer is another idea to control the orientation of the nematic LC. It is generally known as the “command surface”[40,60–62]. A nematic LC cell consists of surface-treated substrates with azobenzene, the homeotropic

alignment of LC can be optically switched to the planar alignment through the *trans*-to-*cis* isomerization of azobenzene on the substrates.

To sum up, the photo-responsive LCs can be achieved by inserting azobenzene derivatives into the LC phase. The characteristics of *trans* azobenzene and *cis* azobenzene have been widely utilized to design new functional photonic LC devices. By applying light with a specific wavelength or certain polarized direction on the azobenzene-containing nematic systems, the scalar order parameter or the alignment of the nematic phase can be easily modulated.

1.4. **Objectives**

Manipulating nanometer-sized impurities with high precision is of importance in the development of tunable photonic structure with nanoscale in LC medium. Until here, we have reviewed the current strategies of manipulating impurities in the nematic phase. The distortion of the LC director field induced by micrometer-sized impurities has been widely studied and has been utilized to drive the manipulation. Yet, the nanometer-sized impurities are not capable to cause the elastic distortion in the LC director field. It is still a challenging issue to find a solution that can manipulate the arbitrary nm-sized impurities, *e.g.* nanoparticles, polymers, and molecules, in the LC medium.

Among the current manipulation strategies, the molecules manipulator offers an effective way to transport the nanometer-sized impurities in the LC since the transportation is guided along the spatial variation of *S* instead of the LC director field. It was reported that the spatial variation of *S* in the nematic phase can be generated by either heating or doping with azobenzene derivatives. Since the special surface-treated substrates that can absorb light are needed to heat the local LC, we can expect that it should be difficult to precisely tune the spatial resolution of *S* in the nematic phase based on the heating. Therefore, dispersing azobenzene derivatives into the nematic phase becomes a better choice.

The photo-induced spatial variation of *S* induced by *trans*-to-*cis* isomerization could drive the fluorescence polymer in the nematic phase, as previously demonstrated[12]. However, since the *cis*-azobenzene molecules also spontaneously diffuse in the nematic phase, the prototype of the molecular manipulator has a poor spatial resolution of *S*, which obstructs the fine-manipulation. To overcome this problem, we propose the immobilization of azobenzene through polymerization in this thesis. We fabricate the liquid crystal gels (LC gels) and study their photo-induced spatial variation of birefringence. The contents of this thesis are outlined by chapters in the following paragraphs.

Chapter 2 describes a newly observed photo-response in the LC gels under UV light. Unlike the conventional photo-induced decrease of Δn in the azobenzene/nematic mixture, an increase of Δn appears under UV irradiation in the LC gels. To elucidate the anomalous increase of Δn, the photo-induced change of Δn and the morphology of the copolymer microstructure are investigated with the variant composition of LC gels. We find that the microstructure of the azobenzene-containing copolymer is important in photo-response of the liquid crystal gels. A mechanism is proposed to explain the anomalous increase of Δn.

Chapter 3 describes the high resolution of photo-induced spatial variation of S in the LC gels via the immobilization of azobenzene. We tune the composition of LC gels to eliminate the anomalous increase Δn, as discussed in Chapter 2, and evaluate the spatial resolution of the LC gels. The photo-induced spatial variation of Δn of the non-polymerized and the polymerized samples are quantitatively compared through measuring their full-width-at-half-maximum (FWHM). We find that the photo-induced change of S, which is linearly proportional to Δn, can be highly constrained in the irradiated area in the polymerized sample.

Chapter 4 summarizes the results and findings of this thesis.

Chapter 2 Photo-induced recovery of liquid-crystalline order with azobenzene-containing copolymer in nematic liquid crystal

To solve the poor resolution of the molecule manipulator, we immobilize the azobenzene through polymerization in the nematic phase, fabricating an LC gel with phase-separation of azobenzene-containing copolymer microstructure. However, unlike typical photo-induced decrease of birefringence (Δn), an increase of Δn appears under UV irradiation in the LC gels. In this chapter, to elucidate the anomalous increase of Δn, we study the photo-induced spatial variation of Δn with various compositions of the LC gels and directly observe the copolymer microstructure through a scanning electron microscope (SEM). We find that the photo-stimulated isomerization of azobenzene reduces the surface anchoring on the copolymer microstructure, which influences the LC director and causes a lower background birefringence before the UV irradiation. We conclude that the weakened anchoring of the copolymer microstructure leads to a recovery of the liquid-crystalline order. Hence, the LC director recovers the uniform orientation of the LC director and reveals the increase of Δn.

2.1. LC gels and experimental set-up

In this section, we introduce the fabrication of LC gels, which is similar to the method in polymer-stabilized-liquid-crystals (PSLCs). The characteristics of the PSLCs are described in 2.1.1 and the details of the preparation of LC gels are described in 2.1.2. The setup and the analyzed method of measuring the photo-induced spatial variation of Δn in LC gels are presented in 2.1.3 and 2.1.4.

2.1.1. Background of polymer-stabilized-liquid-crystals

The preparation of the LC gel was similar to the method in polymer-stabilized-liquid crystals (PSLCs). PSLCs is referred to as the material that dispersing reactive monomers (usually with the concentration of smaller than 10 wt%) into the LC phase followed by photo-polymerization[63,64]. The photo-reactive monomers usually contain acrylate or methacrylate functional groups on both sides in their chemical structures[63]. The orientation of LC influences the diffusion of monomers during the polymerization, leading to the formation of a fibril-like, anisotropic polymer network in the LC phase. The polymer network tends to stabilize the original texture of liquid crystal where they formed in and can be used to improve the electro-optical performance of LC devices[63]. The PSLCs has been developed in the early stage with the nematic phase, and then subsequently extended to various types of LC phases, such as cholesterics and ferroelectric liquid crystals[64–66].

The morphology of the polymer network formed in the nematic phase was dependent on some factors, such as monomer solubility[67], monomers structure[68], polymerization conditions[69], and could greatly affect the electro-optic properties of PSLC devices[63,69,70]. It had been reported that these polymer networks could influence the nearby LC molecules and even show a residual birefringence after the nematic-isotropic phase transition[71,72]. The interaction between the polymer network and the liquid crystal has been discussed by several groups. Fung *et al.* studied the residual birefringence found in PSLCs[71]. In their study, the effect polymer network on the ordering of the liquid crystal is treated as a surface anchoring. A term of surface coupling was supplemented into Landau-de Gennes expression for the free energy density to analyze the orientational order parameter in PSLCs. Similarly, Kraig *et al.* experimentally studied the effect of the polymer on the residual nematic order and theoretically modeled the system[72]. They introduced a spatially varying field to describe the interaction between polymer networks and LC. The forming

polymer fibrils in the nematic phase could reduce or remove the discontinuity in S as the temperature is raised, leading to the vanishing of the first-order phase transition. Ma *et al.* studied the field-induced-reorientation (as commonly known as Fréedericksz transition) in PSLCs[70]. They used a bundle model to describe the polymer fibril formed in the nematic phase. The surface of the polymer bundles had a surface anchoring that imposed an orientation on the liquid crystal molecules. They reported that the transition was profoundly influenced by the morphology of the polymer network. Krossyrev *et al.* also analytically studied the aligning effect of polymer networks on Fréedericksz transition in PSLCs[73]. They used a model that the polymer fibrils formed director domains, which had a finite anchoring on each virtual surfaces, and used Frank elastic theory to study the relationship between the concentration of polymer network and the critical field of reorientation. Yang *et al.* proposed a phenomenological theory to describe the aligning effect of polymer networks in PSLCs[74]. The polymer network that is formed in the nematic phase tends to anchor the local liquid crystal molecules to their longitudinal direction. Their model could provide a good prediction for driving voltage and response time of in the PSLC devices with variant concentration of polymer.

To conclude, the characteristics of PSLCs devices is highly related to the interaction between the liquid crystal and the polymer network. The previous studies suggested that the polymer fibril formed in the nematic phase tends to anchor the local liquid crystal molecules to a direction, which can be treated as surface anchoring at the interface between the polymer domain and the LC medium. Accordingly, the polymer network with a large surface to volume ratio in the LC phases leads to the change in the electric-optical properties of the LC devices.

2.1.2. Preparation of the LC gels

In the present study, the azobenzene methacrylate monomer 11-[4-(4-Butylphenylazo)phenoxy]undecyl methacrylate (Azo-M, purchased from TCI) was mixed with the diacrylate monomer 1,4-Bis-[4-(3-acryloyloxypropyloxy)benzoyloxy]-2-methylbenzene (RM257, purchased from DIC), and the photo-initiator 2,2-Dimethoxy-2-phenylacetophenone (DMPA, purchased from TCI) in nematic liquid crystal 4-Cyano-4'-heptylbiphenyl (7CB, purchased from Merck). The concentration of Azo-M and DMPA were fixed at 3 wt% and 0.5 wt% respectively, whereas that of RM257 was varied from 0 wt% to 2 wt%. Details of their chemical structures were shown in **Fig. 2.1**. The mixture was filled into a quartz cell which was made by sandwiching two planar-rubbed quartz plates with PET spacers of 25 μm. The mixture was polymerized at the nematic phase (T = 36 ℃). The polymerization process was triggered by short-wavelength UV (λ = 254 nm, AS ONE SLUV-8, 1 mW/cm^2, 15 hrs.), which is inert for the trans-to-cis isomerization by avoiding the π-π* absorption of *trans*-azobenzene[44].

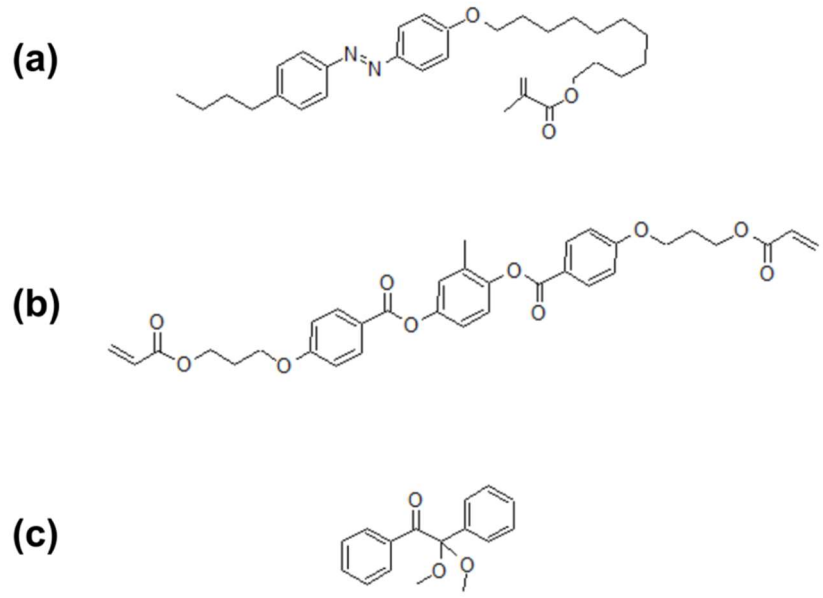

Fig. 2.1 The chemical structures of (a) the azobenzene methacrylate monomer, Azo-M, and (b) the diacrylate monomer, RM257. The two monomers were mixed with (c) the photo-initiator DMPA and then introduced into the nematic liquid crystal 7CB.

2.1.3. Experimental Set-up

After the polymerization, a fluorescence microscope equipped an imaging spectrometer was utilized to stimulate the trans-to-cis isomerization of azobenzene and acquire the photo-induced spatial variation of Δn in the LC gel (**Fig. 2.2).** The mercury lamp of the microscope with a fluorescence filter (U-MWU2, Olympus) emitted UV light with λ = 330 - 385 nm. Note that it was non-polarized light, so the photo-induced reorientation of *trans* azobenzene which occurs under linear-polarized UV light was negligible[40,55]. To obtain the spatial variation of Δn, the intensity of transmitted light was measured under crossed Nicols through the imaging spectrometer. The spatial variation of Δn at the dashed line L, as marked in Fig. 1b, was acquired by analyzing the transmittance spectra. Details of the method were

described in subsection 2.1.4. The sample was kept at T = 36 ℃ by a temperature-controlled stage (Linkam LK-600PH) during the experiment. The irradiated area (**Fig. 2.3 upper**) is confined by a field iris diaphragm and has a diameter of ~ 200 μm. The distribution of light **(Fig. 2.3 lower**) at the dashed line L was measured by using a fluorescence sample (Nile red 0.1 wt% dissolved in 7CB) with a fluorescence filter (U-MNG2, Olympus). The Nile red is a hydrophobic dye which is strongly fluorescent in the nematic phase[75].

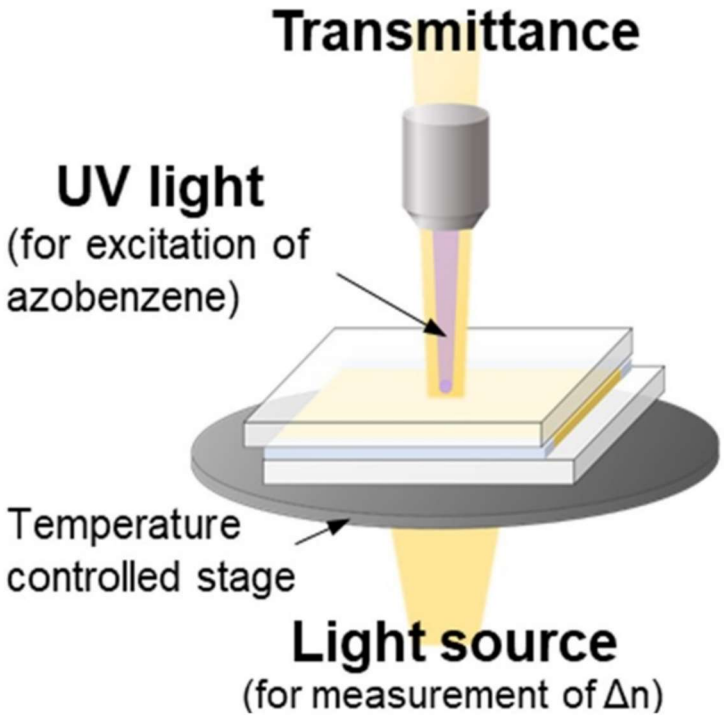

Fig. 2.2 The schematic illustration of the experiment setup.

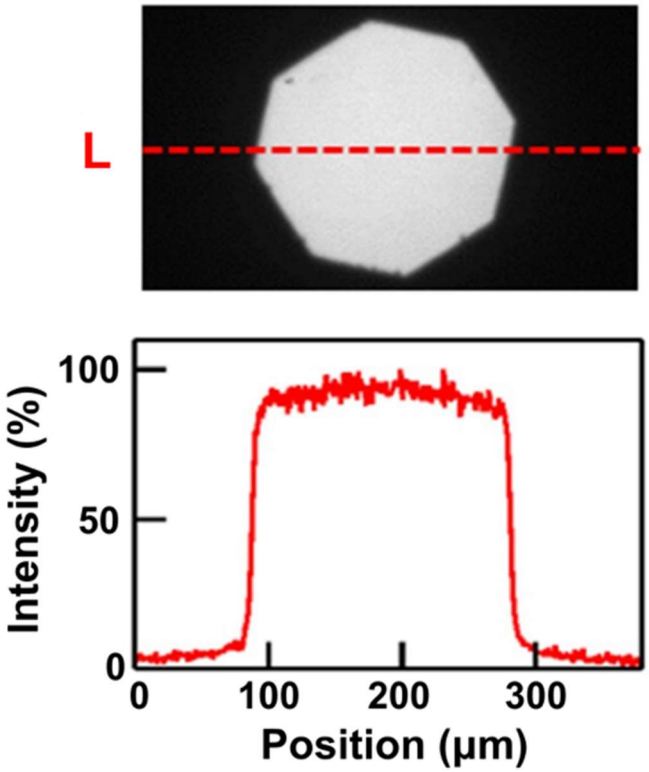

Fig. 2.3 The UV irradiated area with a size of about ~ 200 μm (upper) and the intensity distribution of light at the dashed line L (lower). The dashed line L is represented as the measured position in the birefringence measurement.

2.1.4. Birefringence measurement

In this subsection, we show an example of measuring the photo-induced spatial variation of birefringence. The non-polymerized LC mixture was prepared with Azo-M 3wt% in 7CB and then introduced into a sample cell (purchased from E.H.C., thickness = 25 μm). The monochrome polarized optical microscopy image of the irradiated area is shown in **Fig. 2.4a** after applying UV irradiation on the sample cell (exposure time: 1 min, power: 2.8 mW/cm^2). The circular pattern in the center was corresponding to the irradiated area, where the photo-induced decrease of birefringence resulted in a change of color. Transmittance spectra of the

positions at the dashed line, as marked in **Fig. 2.4a**, was acquired by an imaging spectrometer. As shown in **Fig. 2.4b**, the spectra image indicated that blue-shift appeared in the irradiated area. We picked up two positions in the spectra image (position 1 and position 2) to demonstrate the fitting method of calculating the photo-induced spatial variation of birefringence. The transmittance spectra of position 1 and position 2 were represented as the red open circles and blue open triangles, respectively in Fig. 2a. The transmittance was given by the expressions:

$$T(\lambda) = \mathrm{B}\sin^2\left(\frac{\pi\Delta n \mathrm{d}}{\lambda}\right) + \mathrm{y}_0,$$

$$\Delta n(\lambda) = \mathrm{n}_0 + \frac{\mathrm{n}_1}{\lambda^2}, \quad (1)$$

where B is the amplitude of spectra, d is the cell thickness, y_0 is the offset of spectra and $\Delta n(\lambda)$ is the dispersion relation of the LC with constants n_1 and n_2[12,18]. Here we simply assume d = 25 μm for the commercial product. For the hand-made quartz cells in the main experiment, the real thickness is determined by measuring the interference pattern of the empty cells. The fitting results of $T(\lambda)$ and $\Delta n(\lambda)$ of position 1 and position 2 were plotted in **Fig. 2.5a** and in **Fig. 2.5b**, respectively. By this means, after fitting the transmittance spectra of all positions on the dashed line, we could obtain the spatial variation of Δn under the UV illumination by picking λ = 590 nm as an example wavelength (**Fig. 2.5c**).

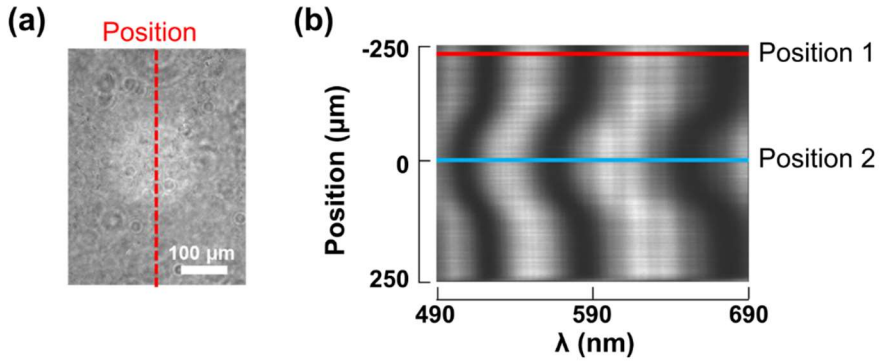

Fig. 2.4 (a) The monochrome polarized optical microscopy image of non-polymerized LC mixture (Azo-M 3 wt% in 7CB) after UV irradiation. (b) The spectra image obtained by an imaging spectrometer.

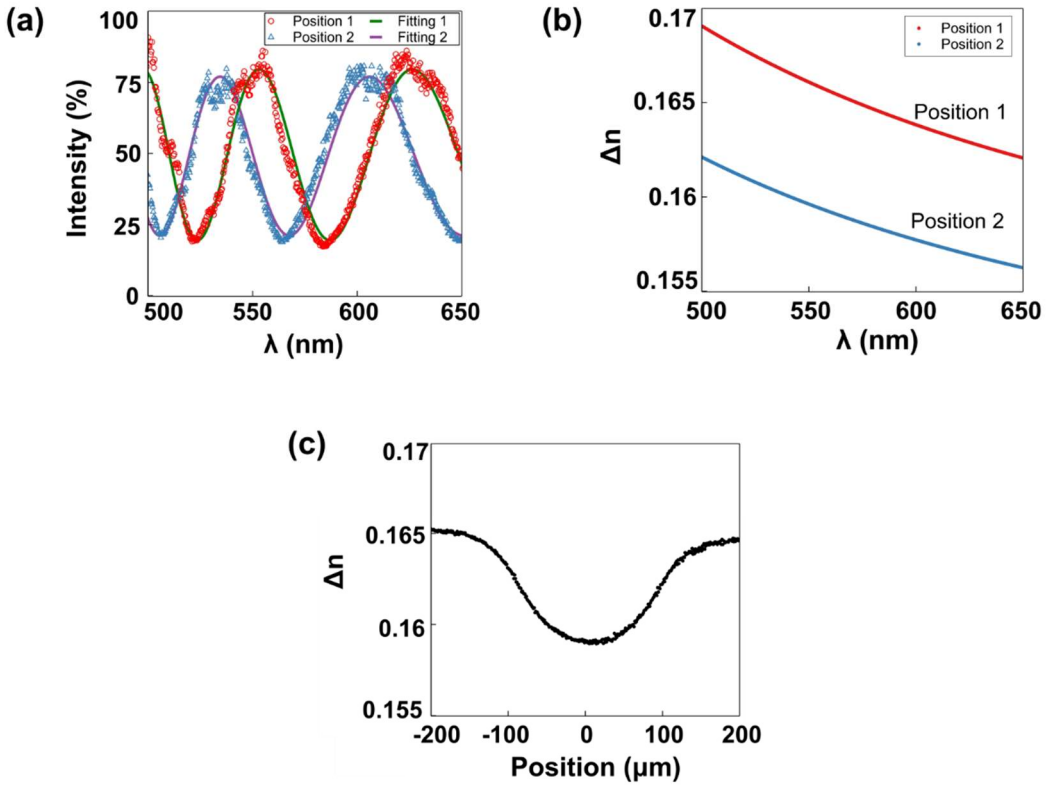

Fig. 2.5 (a) The transmittance spectra at positions: position 1 and position 2. The open symbols are the experimental data and the lines are the fitting results. (b) The fitting results of $\Delta n(\lambda)$ at position 1 and position 2. (c) The spatial variation of Δn under the UV illumination was obtained by choosing $\lambda = 590$ nm.

2.2. **Photo-induced increase of Δ*n* in the LC gels**

After the LC gel was fabricated through the polymerization process, we apply UV light on it to induce the *trans*-to-*cis* isomerization of azobenzene and study its photo-induced spatial variation of Δ*n*. The anomalous increase of Δ*n* is observed during the UV irradiation. To confirm the relation between the isomerization of azobenzene and the increase of Δ*n*, the relaxation behaviors of the increase of Δ*n* are investigated in this section. We also find that the photo-induced change of Δ*n* is dependent on the UV exposure energy, which is related to the generated population of the *cis* isomer.

2.2.1. Photo-induced spatial variation of Δn during UV irradiation

The photo-induced spatial variation of Δ*n* in the LC gel was measured with variant UV exposure time and shown in **Fig. 2.6**. Under the UV light, the Δ*n* first gradually increased in the irradiated area. After the exposure time of 15 s, it started to reverse and decreased at 30 s. It finally became lower than the initial state with the exposure time of 40 s, which was the normal response of azobenzene/nematic LC mixture as we previously introduced. To the best of our knowledge, it was the first time to observe the increase of Δ*n* in the azobenzene/nematic LC mixture under UV irradiation.

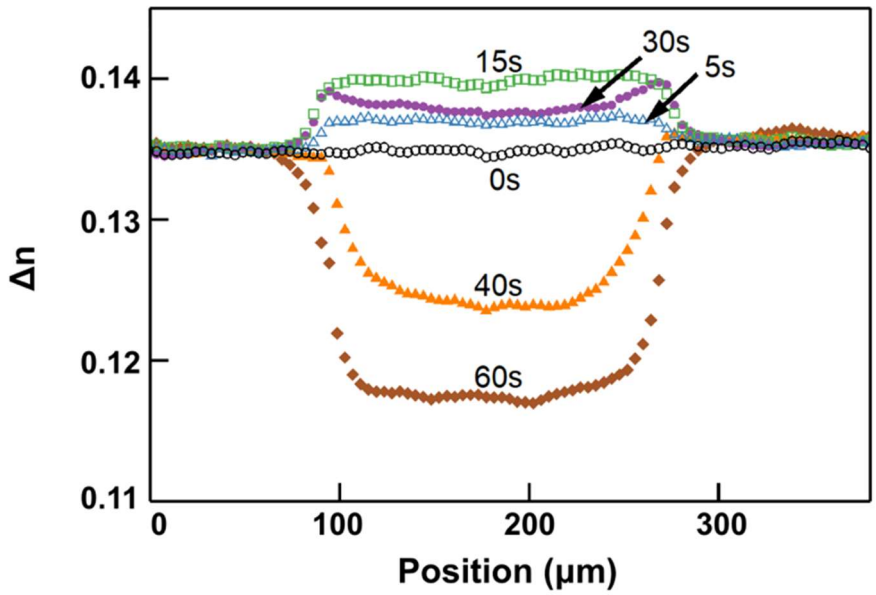

Fig. 2.6 The spatial variation of Δn as a function of UV exposure time (Sample: Azo-M 3 wt%, RM257 1.5 wt%, UV power: 1.6 mW/cm^2 measuring after 20x objective lens).

2.2.2. The relation between the increase of Δn and the isomerization of azobenzene

We first confirm the relation between the anomalous increase of Δn and the isomerization of azobenzene. After the increase of birefringence (Δn-Δn_0, where Δn_0 is the initial state) appeared under UV irradiation (**Fig. 2.7** black filled circles), the UV light was turned off and replaced by blue light (λ = 460 - 495nm, 38 mW/cm^2) to induce *cis*-to-*trans* isomerization. The increase of Δn was quickly removed and restored to the initial value within 5 s (**Fig. 2.7** blue open circles). On the contrary, after the UV light was turned off without the irradiation of blue light, the increase of Δn in the irradiated area (= $(\Delta n$-$\Delta n_0)_a$, the averaged Δn-Δn_0 of the irradiated area, as marked in **Fig. 2.7**) gradually decreased, and finally restored to Δn_0 after a long time (**Fig. 2.8**).

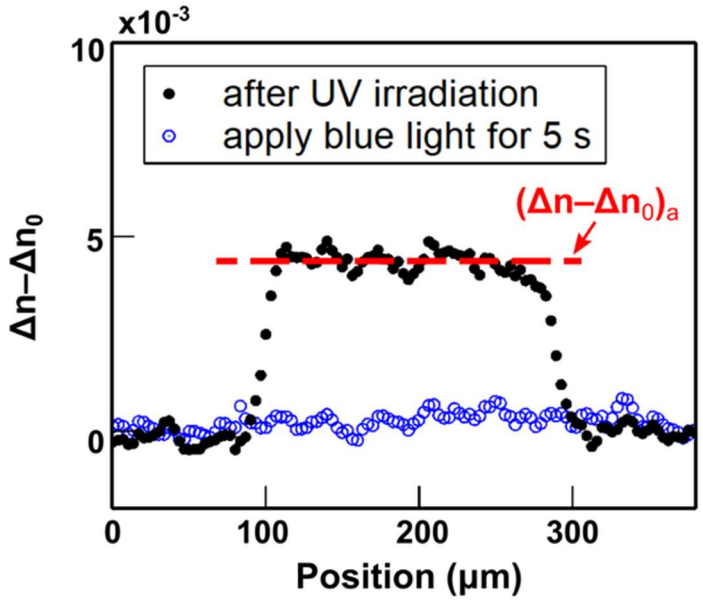

Fig. 2.7 The increase of Δn can be removed by applying blue light after switching off UV light, where Δn_0 is the initial state (Azo-M = 3 wt%, RM257 = 1.5 wt%).

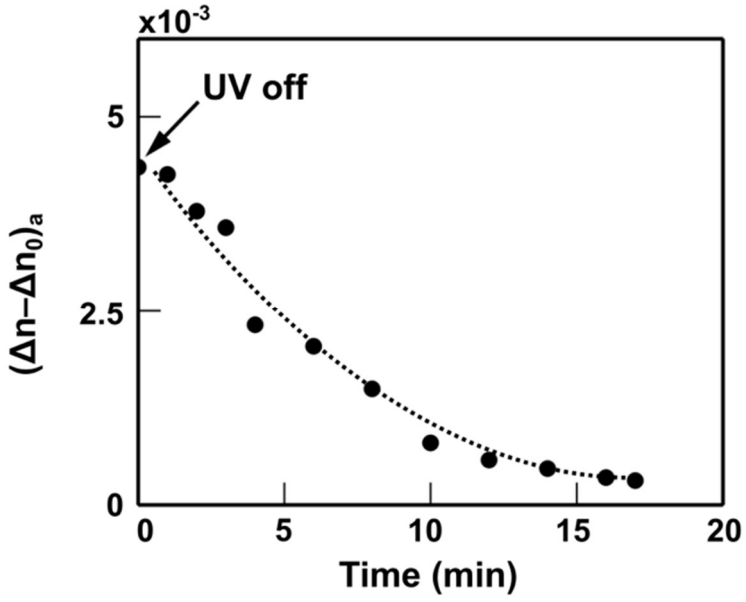

Fig. 2.8 The relaxation behavior of the increase of Δn without applying blue light, where $(\Delta n\text{-}\Delta n_0)_a$ is the averaged $\Delta n\text{-}\Delta n_0$ of the irradiated area (Azo-M = 3 wt%, RM257 = 1.5 wt%).

From the results of **Fig. 2.7** and **2.8**, we can conclude that the anomalous increase of Δn was directly originated from the *trans*-to-*cis* isomerization of azobenzene. Because the *cis*-azobenzene slowly converted back to the *trans* form through the thermal relaxation, while the blue light accelerated the *cis*-to-*trans* isomerization due to the irradiation in the n-π* absorption band of cis azobenzene.

2.2.3. Photo-induced change of Δn *under variant UV exposure energy*

The photo-induced change of Δn to the UV exposure time was also plotted with variant UV power (**Fig. 2.9a**). The curves of $(\Delta n\text{-}\Delta n_0)_a$ could match perfectly after setting the x-axis to the UV exposure energy instead of the UV exposure time (**Fig. 2.9b**). Therefore, the photo-induced change of Δn was dependent on the UV exposure energy, which was related to the generated *cis* azobenzene in the irradiated area. The population of *cis* azobenzene should increase with the UV exposure energy due to the slow thermal *cis*-to-*trans* isomerization process (**Fig. 2.8**). We calculated the $(\Delta n\text{-}\Delta n_0)_a$ of **Fig. 2.6** and plotted it with various UV exposure energy, as shown in **Fig. 2.10**. The increase of $(\Delta n\text{-}\Delta n_0)_a$ was saturated at an exposure energy of ~ 0.03 (J/cm^2). It reversed and became lower than the initial state with the increase of exposure energy, indicating that the anomalous increase of Δn disappeared with a major amount of *cis* population.

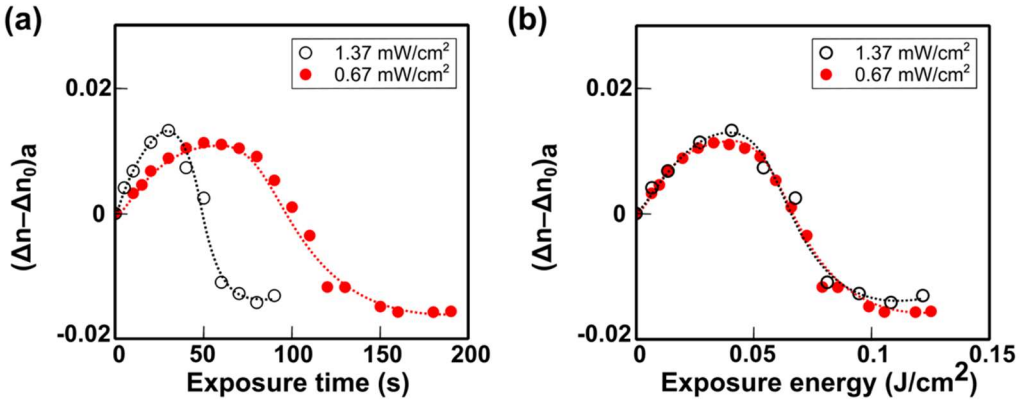

Fig. 2.9 (a)The photo-induced increase of Δn (= $(\Delta n\text{-}\Delta n_0)_a$, the averaged $\Delta n\text{-}\Delta n_0$ of the irradiated area, where Δn_0 is the initial state) in various UV exposure time, where the open circles and red filled circles represent the UV power of 1.37 mW/cm^2 and 0.67 mW/cm^2, respectively. (b) The $(\Delta n\text{-}\Delta n_0)_a$ in (a) is replotted as a function of UV exposure energy (sample: Azo-M = 3 wt%, RM257 = 1.5 wt%).

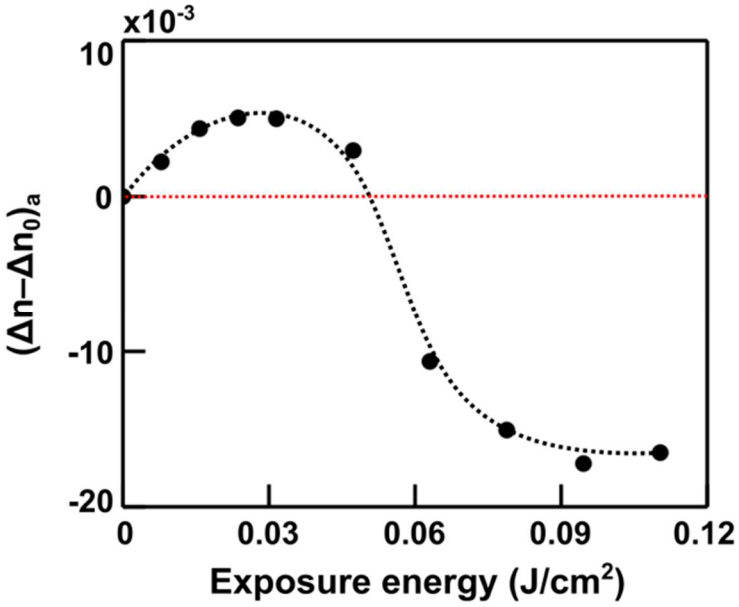

Fig. 2.10 $(\Delta n\text{-}\Delta n_0)_a$ to various UV exposure energy (Azo-M = 3 wt%, RM257 = 1.5 wt%).

2.3. **Effects of monomer ratio on the photo-induced change of Δ*n***

In this section, we prepared the LC gels for the different mass ratios of RM257 to Azo-M ($r_{R/A}$) with fixing Azo-M = 3 wt% to study how the increase of Δ*n* influenced by the composition of LC gels.

Fig. 2.11 shows the polarized optical microscopy (POM) images for $r_{R/A}$ = 0 ~ 0.5. The circular phase separation regions appeared at $r_{R/A}$ = 0 and then disappeared with the increase of $r_{R/A}$. The textures looked uniform as $r_{R/A} \geqq 0.33$. These LC gels with a higher value of $r_{R/A}$ kept the alignment as same as the original alignment before the polymerization. The predominant director of LC still oriented along the rubbing direction. The $(\Delta n\text{-}\Delta n_0)_a$ versus UV exposure energy was measured with $r_{R/A}$ from 0 to 0.67 (**Fig. 2.12**). The photo-induced change of Δ*n* was found to significantly depend on $r_{R/A}$. At $r_{R/A}$ = 0, it showed a monotonic decrease of Δ*n* with the increase of exposure energy. The strong increase of Δ*n* was found at $r_{R/A}$ = 0.33. The maximum value of the anomalous increase decreased with further addition of RM257. At $r_{R/A}$ = 0.67, the $(\Delta n\text{-}\Delta n_0)_a$ values were monotonically decreasing with the increase of exposure energy again.

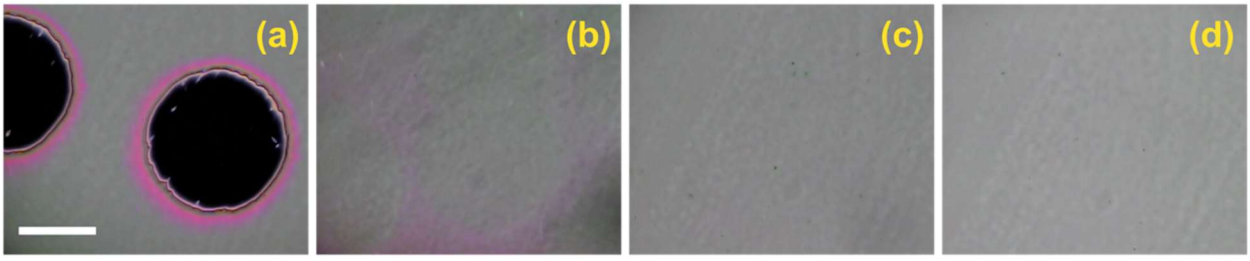

Fig. 2.11 The POM images after polymerization of $r_{R/A}$ = (a) 0, (b) 0.17, (c) 0.33 and (d) 0.5 (scale bar: 150 μm).

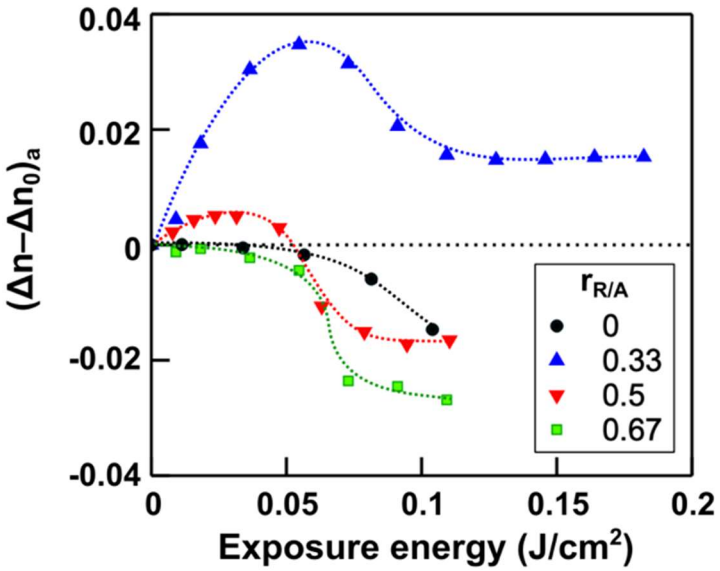

Fig. 2.12 The relation between the $(\Delta n\text{-}\Delta n_0)_a$ of $r_{R/A}$ from 0 to 0.67 and the UV exposure energy.

Not only the photo-induced change of Δn, but the background birefringence of the LC gels was also dependent on $r_{R/A}$. The birefringence before UV irradiation, Δn_0, was measured for $r_{R/A}$ ranging from 0 to 0.67 and shown in **Fig. 2.13**. The deterioration of birefringence at $r_{R/A} = 0$ could be attributed to the appearance of the phase separation domains as confirmed in POM image, where these regions were already turned into isotropic phase (**Fig. 2.11** upper). On the other hand, at $r_{R/A}$ = 0.33, 0.5, 0.67, which had no obvious phase separation in the POM images, the Δn_0 values increased near to the Δn_0 of pure 7CB (dashed line in **Fig. 2.13**) with the increase of $r_{R/A}$. Since the presence of nano-sized impurities in the nematic phase could reduce the scalar order parameter[12], we measured the Δn_0 of non-polymerized LC mixtures to verify how the Δn was influenced by the non-polymerized monomers. The Δn_0 values were 0.155 for $r_{R/A}$ = 0.67 (Azo-M = 3 wt%, RM257 = 2 wt%), and 0.154 for $r_{R/A}$ = 0

(Azo-M = 5 wt%, RM257 = 0 wt%). Therefore, according to Δn_0 = 0.156 of pure 7CB, we could neglect the decrease of Δn_0 originated from the non-polymerized monomers remained in the LC gels. The decrease of Δn_0 in the LC gels should relate to the formation of copolymer microstructure through the polymerization.

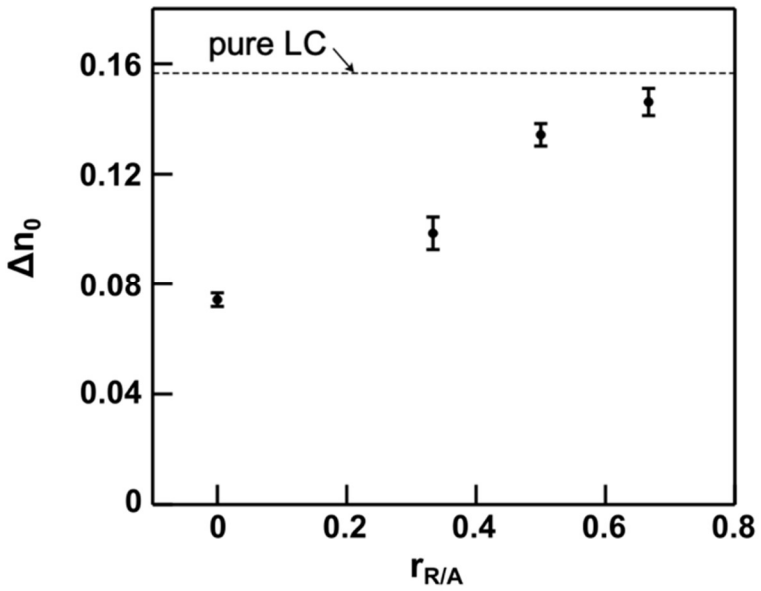

Fig. 2.13 The background birefringence (Δn_0) of the LC gels with variant $r_{R/A}$ before UV irradiation. The dashed line is Δn_0 of pure 7CB.

2.4. **Origin of the decrease of Δn_0**

In section 2.3, the results indicated that the photo-induced change of Δn and the background birefringence Δn_0 were dependent on the mass ratio $r_{R/A}$. We found that the LC alignment of the LC gels with $r_{R/A} \geqq 0.33$ was still oriented to the rubbing direction after the polymerization process, while these gels had lower values of Δn_0 comparing to that of the pure 7CB. In this section, to investigate the origin of the deterioration of Δn_0, the copolymer microstructure of the gels is directly observed through a scanning electronic microscope (SEM). Based on the SEM images, we propose a hypothesis to explain the decrease of Δn_0.

2.4.1. Copolymer microstructures observed by scanning electronic microscope (SEM)

To investigate the origin of the decrease of Δn_0, the microscopic copolymer structures for the LC gels with $r_{R/A} \geqq 0.33$, which showed the uniform orientation under POM observation, were investigated by SEM. The cells were dismantled and immersed into hexane for 5 min to remove the LC media in between the copolymer structures. The copolymer structures were left on the quartz plates and coated by Pt (thickness ~7 Å) for observation of SEM. **Fig. 2.14a – 2.14c** are the copolymer structures of $r_{R/A}$ = 0.33, 0.5 and 0.67 respectively. The copolymer fibrils were found for both $r_{R/A}$ = 0.33 and 0.5. The fibrils with a serrated shape appeared at $r_{R/A}$ = 0.33 (**Fig. 2.14a**), whereas the fibrils had a smoother shape at $r_{R/A}$ = 0.5 (**Fig. 2.14b**). The thickness of fibrils was ranging from 0.2 ~ 0.5 μm, which had a similar dimension with the polymer fibrils formed in PSLCs[67,71]. At $r_{R/A}$ = 0.67, the copolymer droplets with a diameter of 0.5 ~ 2.5 μm appeared instead of the fibrillar structures (**Fig. 2.14c**).

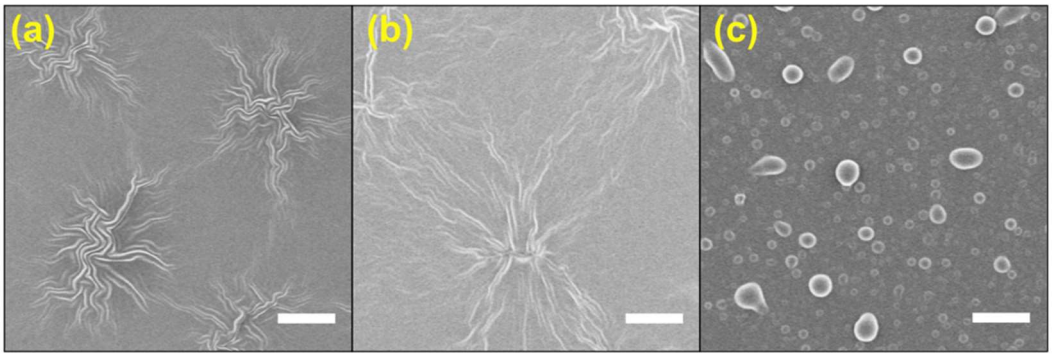

Fig. 2.14 The SEM images of copolymer microstructure left on the quartz plates, where $r_{R/A}$ = (a) 0.33, (b) 0.5 and (c) 0.67 (scale bars: 5 μm, rubbing direction: from up to down).

2.4.2. The hypothesis of the decrease of Δn_0

Based on this observation, we suggest the hypothesis of the decrease of Δn_0 in the LC gels as follows. The surface of the copolymer fibrils had a finite anchoring strength, as reported in PSLCs[70,71,74] and confined LC systems[76], and imposed an orientation on the local LC molecules. The randomly oriented copolymer fibrils locally distorted the original uniform LC director, resulting in the decrease of averaged Δn. Thus, the decrease of Δn_0 was not related to the change of the scalar order parameter. It was attributed to the distorted LC director field through the microscopic copolymer structure. Accordingly, the large decrease of Δn_0 appeared in the LC gels of $r_{R/A}$ = 0.33 because of the large distortion from serrated fibrils. Increasing of $r_{R/A}$ to 0.5 resulted in the smoother fibrils and thus the distortion was weakened. When $r_{R/A}$ increased to 0.67, Δn_0 recovered to near the original value of 7CB since the distortion diminished with the absence of microscopic fibrils.

2.5. **Changes of surface anchoring under UV irradiation**

According to the hypothesis of the decrease of Δn_0 in section 2.4, we expect that the mechanism of the anomalous increase of Δn should be related to the change of the surface anchoring on the copolymer fibrils under UV illumination. In this section, we quantitatively studied the anchoring strength of the LC gels via a magnetic-field-induced orientation of LC measurement.

The magnetic field was applied perpendicularly to the rubbing direction of the LC gels to induce the Fréedericksz transition. The threshold of the Fréedericksz transition is determined by measuring the transmitted light under crossed Nicols, where the rubbing direction is parallel to the analyzer. Usually, for the homogeneous cell with a thickness of 25 μm which satisfied the Mauguin condition[16], it should remain dark under the magnetic field because of the strong anchoring of the alignment layers on the substrates. For the LC gels, we can observe the magnetic-field-induced change in transmittance. It should be attributed to the copolymer clinging on the planar-rubbed substrates (as shown in SEM images) which weakens the original anchoring strength of the planar-alignment layer. Therefore, with the soft boundary conditions, we can observe an increase of transmittance under the magnetic field. The result is shown in **Fig. 2.15**. After the photo-induced increase of Δn was confirmed through the birefringence measurement, the sample was set in an electromagnetic device to measure the transmittance with different strength of the magnetic field. The threshold was about 200 mT (filled circles) for the UV irradiated LC gel. Then the sample was left for 2 hrs until the azobenzene recovers to the *trans* form. The threshold increased to ~ 220 mT (open circles) after the thermal *cis*-to-*trans* isomerization. The raising of the threshold indicated that the anchoring strength increased after the *cis*-to-*trans* isomerization, i.e., the photo-induced *cis* isomers on the copolymer microstructure resulted in a decrease of anchoring strength.

Similarly, the photo-induced *trans*-to-*cis* isomerization of azobenzene could lead to a weak anchoring strength, which was reported by other group previously[77].

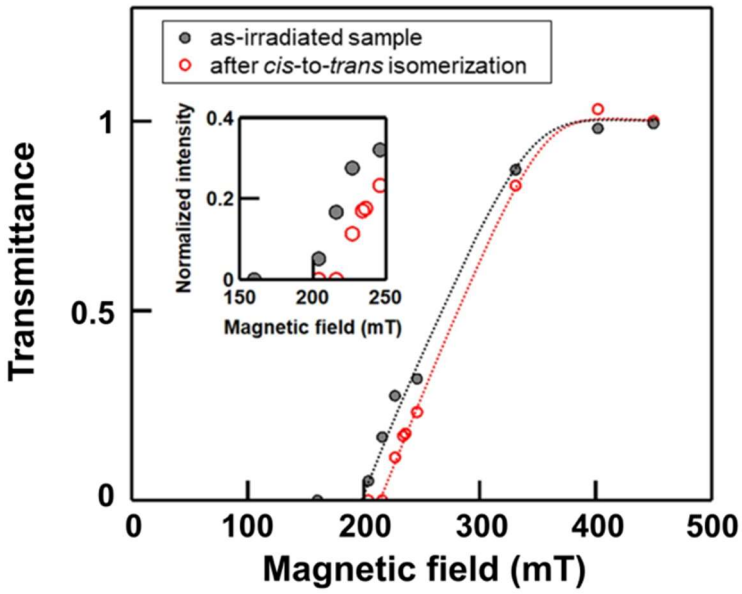

Fig. 2.15 The magnetic-field-induced orientation of LC measurement for the as-irradiated sample and after the thermal relaxation (sample: Azo-M 3 wt%, RM257 1 wt%). The inset is the close-up near the threshold. The photo-induced increase of Δn is confirmed by the birefringence measurement after applying UV light on the whole sample for 5 s (4 mW/cm^2). Each point was measured by applying the magnetic field for 5 s. The lines are a guide for the eye.

2.6. **Mechanism of the increase of Δ*n***

Finally, we conclude the mechanism of the anomalous photo-induced increase of Δ*n* as the following explanation. After the polymerization, the phase separation occurred and the copolymer microstructure formed in the LC medium. The finite anchoring strength on the surface of the copolymer microstructure caused a distortion in the local orientation of LC, leading to a decrease of Δn_0 in the LC gels. This disturbance vanished as the sample had high $r_{R/A}$. Under UV illumination, the generated *cis* isomers weakened the anchoring strength on the copolymer microstructure. The increase of Δ*n* appeared since the distortion in the orientation of LC was diminished. The high value of Δ*n* subsequently started to decrease with the further addition of UV exposure energy. It was because the new-generated *cis* azobenzene disturbed the alignment of the LC molecules. When the major amount of *trans* azobenzene in the irradiated area was converted into *cis* form, the Δ*n* decreased to lower than the initial state. As previously reported, the Δ*n* was proportional to the scalar order parameter *S*, and they both decreased with UV exposure time due to the formation of the *cis* isomer in the azobenzene/nematic LC system[12,30]. Therefore, the scalar order parameter *S* finally decreased with the sufficient concentration of *cis* azobenzene in the LC gels, as the conventional behavior.

2.7. **Summary**

In this chapter, we reported a newly observed photo-response in the LC gel. Our results supported that the anomalous increase of Δn was related to the azobenzene-containing copolymer microstructure. The local distortion in LC originated from the surface anchoring on this copolymer microstructure was reduced by the generation of *cis* azobenzene. Our discovery can provide further functions for current applications, such as manipulation of μm- or nm-sized impurities in the nematic LCs[8,12]. These new findings can help create more designable photo-responsive structures for the fabrication of photonic LC devices.

Chapter 3 Light-driven modulation of scalar order parameter for high spatial resolution

Herein, the immobilization of azobenzene molecules via polymerization serves as a solution to prevent the unfavorable effect from the diffusion of azobenzene. In this chapter, we tune the composition of LC gels to eliminate the anchoring effect of the copolymer microstructure, which was already discussed in Chapter 2, and evaluate the spatial resolution of the LC gels. We quantitatively compare the photo-responses of the LC gels with that of the prototype molecular manipulator under the UV light. Their photo-responses are elucidated by measuring the spatial variation of birefringence (Δn) under UV irradiation. Since Δn is proportional to S [12,72], the full-width-at-half-maximum (FWHM) of the variation of Δn indicates that the photo-induced change of S can retain the feature of stimulating light in the LC gels. We conclude that the LC material for modulating the scalar order parameter with a high spatial resolution has been achieved by our method.

3.1. Material

We prepare non-polymerized and polymerized samples with a fixed concentration of azobenzene-containing monomer to evaluate the improvement of the spatial resolution through our method. Here we provide the details of fabricating these samples and the setup of measuring the photo-induced spatial variation of birefringence.

3.1.1. Preparation of non-polymerized and polymerized samples

The monomers used in this chapter was the same as that in Chapter 2. The azobenzene-containing methacrylate monomer 11-[4-(4-Butylphenylazo)phenoxyundecyl methacrylate

(Azo-M, Tokyo Chemical Industry Co., Ltd.) were mixed with the di-acrylate monomer 1,4-Bis-[4-(3-acryloyloxypropyloxy)benzoyloxy]-2-methylbenzene (RM257, DIC Corporation) and the photo-initiator 2,2-Dimethoxy-2-phenylacetophenone (Tokyo Chemical Industry Co., Ltd.). Their chemical structures were shown in **Fig. 3.1a** and **3.1b**. According to the results from section 2.3 in Chapter 2, we tune the mass ratio of Azo-M to RM257 to be 1:1 to eliminate the abnormal photo-induced increase of birefringence, which we have previously discussed in Chapter 2. The photo-initiator was added with a ratio of 1/10 to the total monomer concentration. The mixture was dissolved in a nematic LC (7CB) and then was applied to a quartz cell. The cell was made of two planar-rubbed quartz plates separated by the PET spacers with a thickness of 25 μm. The preparation of the LC gels was the same as the process mentioned in Chapter 2. The polymerization in the nematic phase was performed by the illumination of short-wavelength UV (λ = 254 nm), which is inert for the *trans*-to-*cis* isomerization of azobenzene (λ = 300 ~ 400 nm). The temperature of the quartz cell was maintained at 36 ℃ (lower than the nematic-to-isotropic transition temperature of the LC mixture, which contains 3 wt % Azo-M and 3 wt% RM257, for 5 ℃) during the polymerization and the following experiment. After the polymerization, the polarized optical microscope image indicated that the predominant director of LC molecules preserved the original direction (**Fig. 3.1c**).

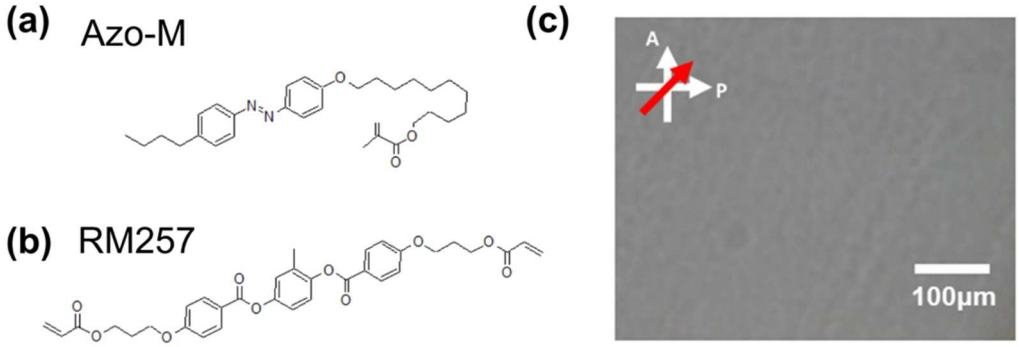

Fig. 3.1 The chemical structures of (a) Azo-M and (b) RM257. (c) A polarized optical microscope image of an as-polymerized sample, where the arrows A, P were the analyzer and polarizer, and the red arrows represented the rubbing direction of the LC cell (Azo-M = 3 wt%, RM257 = 3 wt%).

3.1.2. Setup of measuring photo-induced spatial variation birefringence

The quartz cells containing LC mixture were placed under the fluorescence microscope to measure the photo-induced change of Δn (**Fig. 3.2**). As shown in **Fig. 3.2**, the UV light for the excitation of azobenzene and the visible light for the measurement of Δn were used. Light from the mercury lamp passed through a pinhole, a filter cube M1 (U-MNU2 purchased from Olympus, λ = 330 - 385 nm), and a 20X objective lens O1 to induce the isomerization of azobenzene in the sample. The illuminated area in the sample was visualized by a fluorescence sample and shown in **Fig. 3.3**. An imaging spectrometer set on the top of the microscope received the transmitted light to acquire the transmittance spectra of different positions along the line L, as marked in **Fig. 3.3**. The spatial variation of Δn at L was obtained by fitting the transmittance spectra with the equations (1), as already introduced in the subsection 2.1.4. The distribution of UV light which induced the change of Δn at L was acquired by measuring the fluorescence intensity in **Fig. 3.3**, and was plotted in **Fig. 3.4**. The

x = 0 was defined at the peak of UV light. The profile of light has the FWHM of 16 μm by fitting the distribution with a Gaussian function (red line in **Fig. 3.3)**.

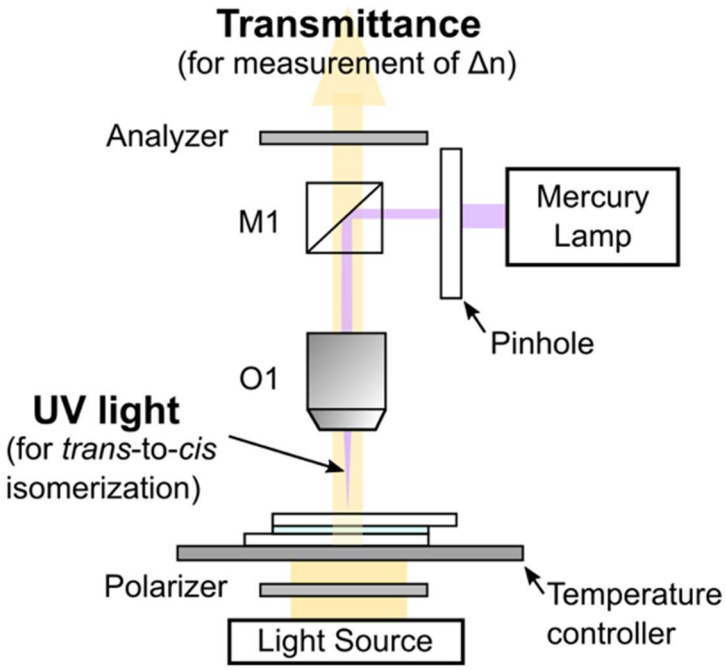

Fig. 3.2 The schematic illustration of the experimental set-up.

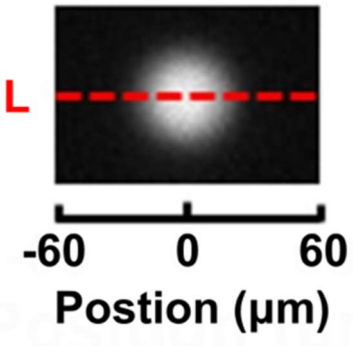

Fig. 3.3 The circular illuminated area visualized by a fluorescence sample. The line L denotes the analyzed positions of the birefringence measurement.

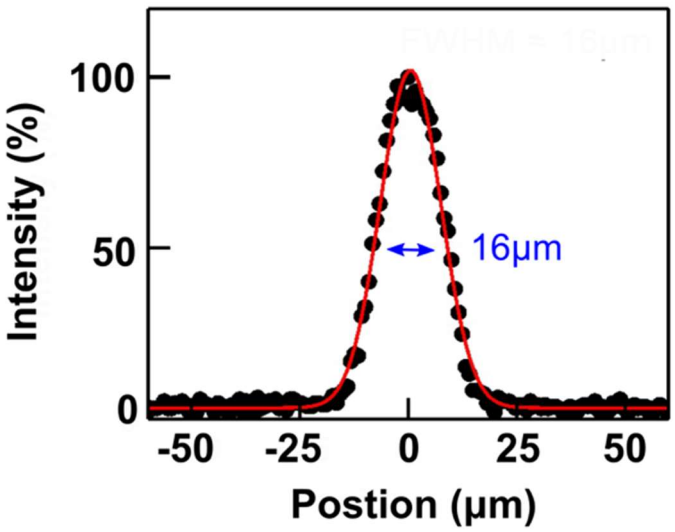

Fig. 3.4 The profile of excitation light obtained at line L.

Here we show an example of acquiring the photo-induced spatial variation of Δn with the UV distribution shown in **Fig. 3.4**. An example of the birefringence measurement of non-polymerized Azo-M 3 wt% dissolved in 7CB is shown in **Fig. 3.5a - 3.5c**. The transmittance spectra images (see **Fig. 3.5a**) were obtained by the imaging spectrometer, which acquired and stacked the transmittance spectra of different positions on the line L, as marked in **Fig. 3.4**. The position-axis are referenced to the position of the UV light, where the peak of the UV light is set to position = 0. The transmittance spectra of position 1 (open circles) and position 2 (filled circles) are shown in **Fig. 3.5b**. The transmittance spectra of the positions along the L are then fitted by the equations (1). As shown in **Fig. 3.5c**, the photo-induced spatial variation of birefringence is acquired by choosing $\lambda = 590$ nm. It should be noted that the thick cell benefits the fitting process. Here, we compare the transmittance spectra images using cells with a thickness of 8 μm and 25 μm, as shown in **Fig. 3.6**. Both cells contained

non-polymerized 3 wt% Azo-M in 7CB. With the thicker cell (25 μm), more periods of peaks could be observed in the CCD vision, and this benefited the fitting process using the equation (1).

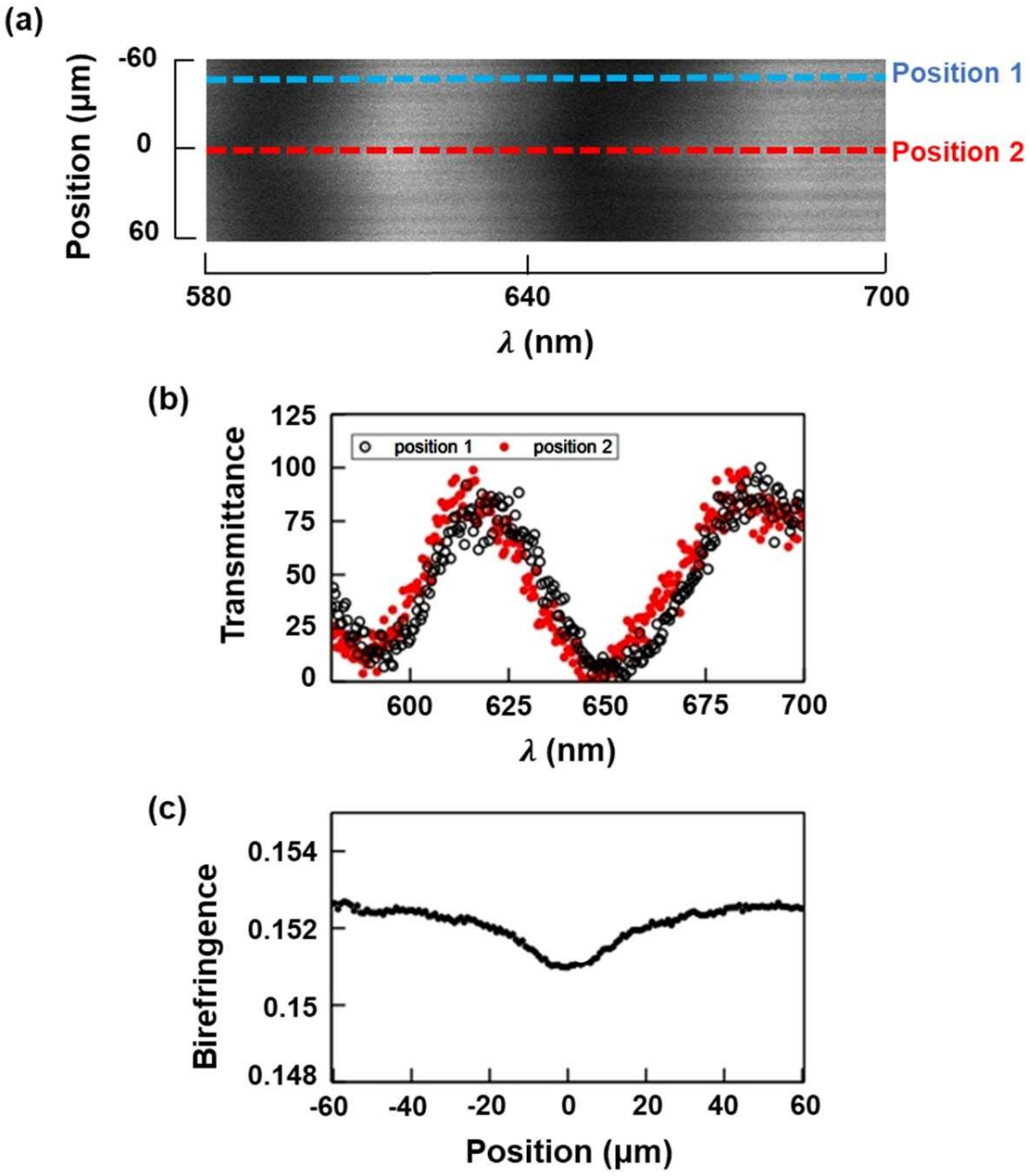

Fig. 3.5 (a) The transmittance spectra images obtained by an imaging spectrometer. (b) The transmittance spectra of position 1 (open circles) and position 2 (filled circles). (c) The photo-induced spatial variation of birefringence.

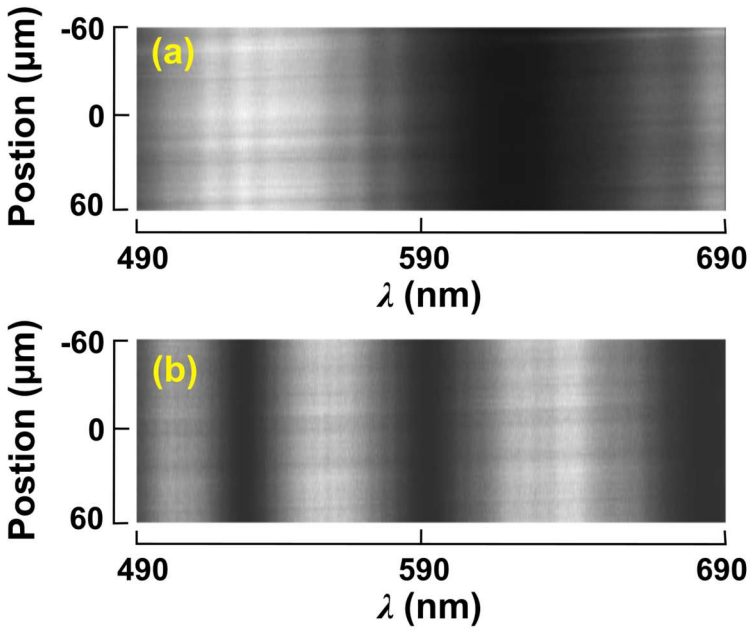

Fig. 3.6 Transmittance spectra images acquired by using cells (commercial products from E.H.C.) with a thickness of (a) 8 μm and (b) 25 μm.

3.2. **The improved spatial resolution via immobilization of azobenzene**

We first compared the photo-induced spatial variation of Δn between the non-polymerized and the polymerized samples with a fixed concentration of Azo-M. The polymerized sample contained 3 wt% Azo-M, 3 wt% RM257, 0.6 wt% photo-initiator, while the non-polymerized sample contained 3 wt % Azo-M without photo-initiator. The resulting spatial variation of Δn of both samples was shown in **Fig. 3.7**. Both Δn of the two samples were normalized by Δn_0, which was the initial state before UV irradiation. The exposure time of UV irradiation (UV power: 2.4 mW/cm2) was controlled to be 40 s. After UV irradiation, the Δn decreased over a broad region (x = -60 μm ~ 60 μm) in the non-polymerized sample (black open circles), whereas the Δn decreased in a narrow region in the polymerized sample

(red filled circles). Furthermore, the amplitude of the photo-induced change of Δn in the two samples was apparently different. The normalized Δn decreased to 0.99 in the non-polymerized sample while that in the polymerized sample decreased to ~ 0.95. The photo-induced spatial variation of Δn was fitted by a Gaussian function:

$$ae^{\frac{-(x-b)^2}{2w^2}} + c, \tag{2}$$

where *a, b, c* and *w* were constants, to acquire FWHM. As noted in **Fig. 3.7**, the FWHM of the non-polymerized sample was 38 μm, and that of the polymerized sample was 14 μm. It suggested that the spatial variation profile of Δn of the polymerized sample was closed to the profile of UV light, which had the FWHM of 16 μm.

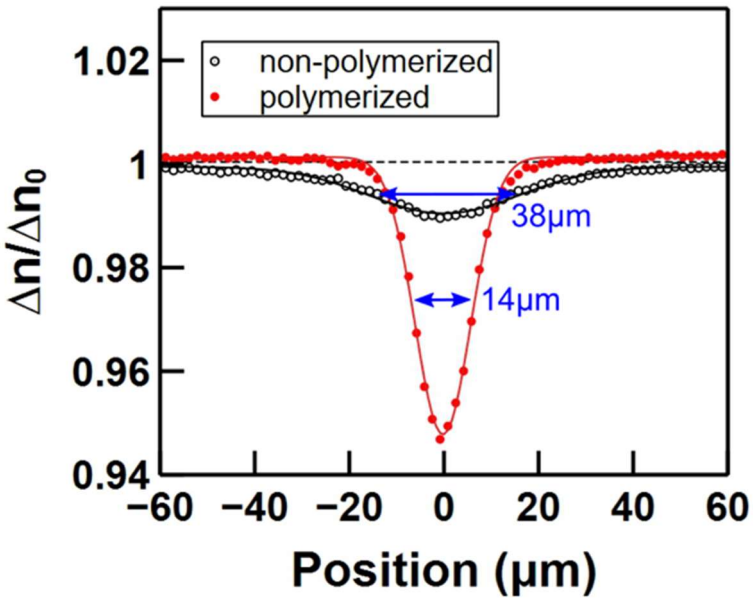

Fig. 3.7 The photo-induced spatial variation of Δn in the non-polymerized sample and the polymerized samples after UV irradiation of 40 s. The red line and the black line represented the fitting results of the Gaussian function.

3.3. **Effects of the diffusion of Azo-M on the photo-induced spatial variation of Δ*n***

3.3.1. Time evolution of the photo-induced spatial variation of Δn

The time evolution of the spatial variation of normalized Δ*n* was investigated to observe the diffusion of Azo-M in the non-polymerized and the polymerized samples. A fixed concentration of Azo-M (3 wt%) was used. The normalized Δ*n* of the two samples under UV irradiation with variant exposure time were shown in **Fig. 3.8a** and **3.8b**. In the non-polymerized sample, Δ*n* first started to decrease in the center of the illuminated area at t = 10 s. Outside the illuminated area, the decrease of Δ*n* could be also observed at t = 30 s. The normalized Δ*n* gradually decreased in a wide region with increasing UV exposure time. On the other hand, the decrease of Δ*n* developed faster in the polymerized sample. In the center of the illuminated area, the normalized Δ*n* greatly decreased with the increase of the exposure time. Comparing to the large decrease of Δ*n* at the center, the decrease of Δ*n* outside the illuminated area was almost negligible.

To quantitatively compare the above results, the spatial variation of Δ*n* in **Fig. 3.8a** and **3.8b** were analyzed for the information of the FWHM. As shown in **Fig. 3.9**, the FWHM of the non-polymerized sample apparently increased with the exposure time, while the FWHM of the polymerized sample retained the value almost close to the FWHM of UV light.

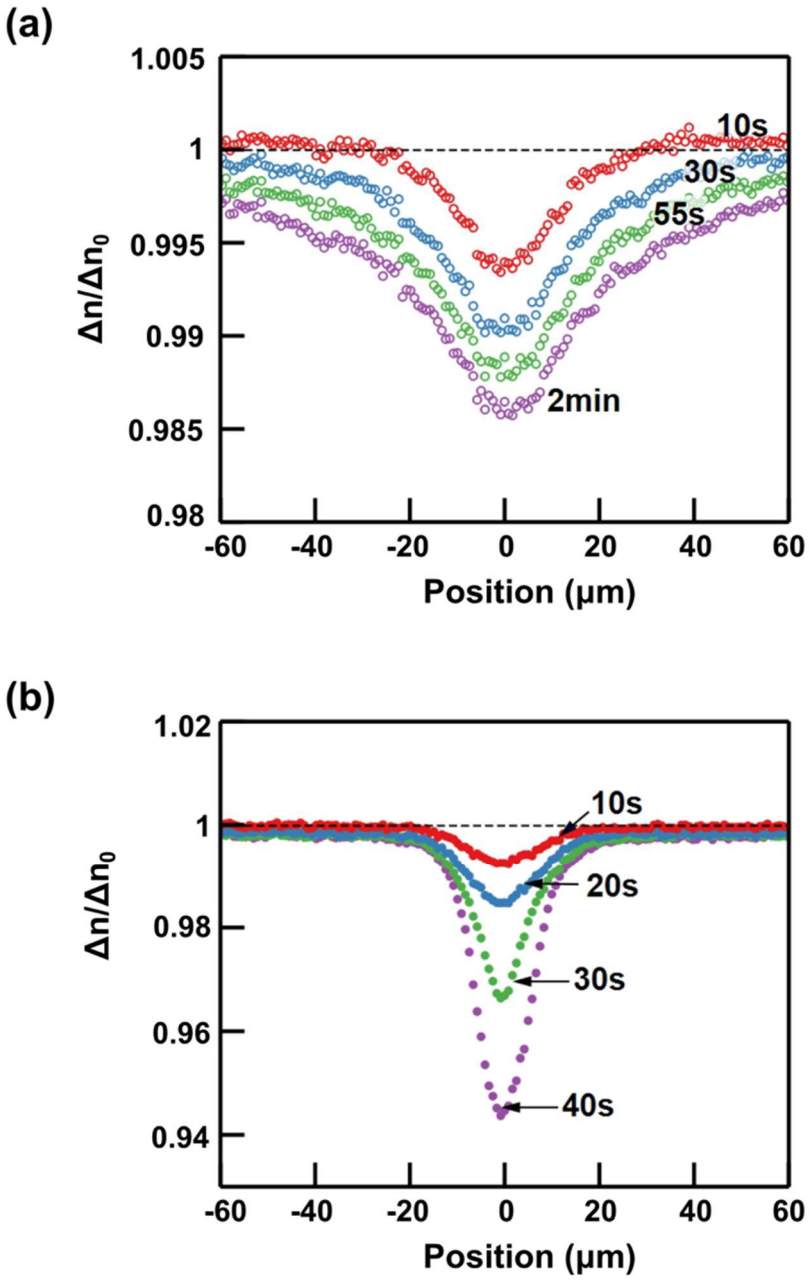

Fig. 3.8 Comparison of the photo-induced spatial variation of Δn between the non-polymerized and the polymerized sample under variant UV exposure time (power: 2.4 mW/cm^2): the normalized Δn of (a) the non-polymerized sample and (b) the polymerized sample.

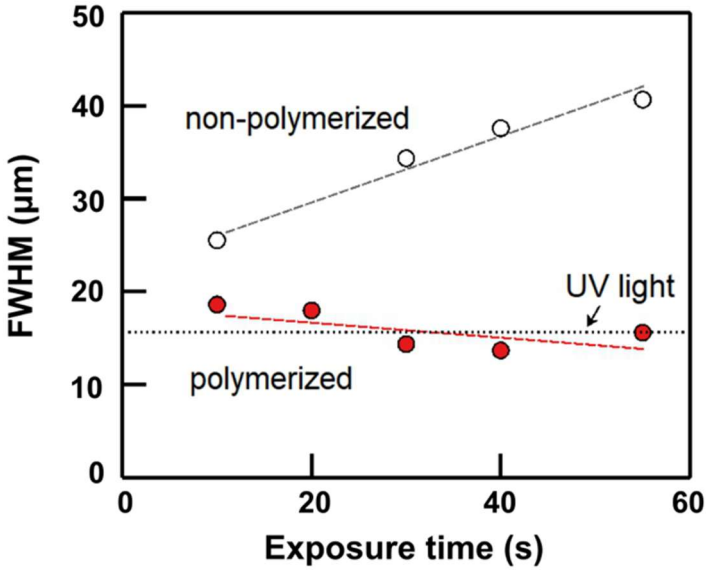

Fig. 3.9 FWHM as a function of UV exposure time. The dotted line is the FWHM of UV light.

According to **Fig. 3.8** and **Fig 3.9**, we proposed the following mechanism. Under UV irradiation, the *cis*-azobenzene monomers are generated in the illuminated area in the non-polymerized sample. The *cis* isomer diffused with time and expanded the affected LC area. Thus, the broadening FWHM appeared in the non-polymerized sample. On the contrary, since the azobenzene group was embedded in the polymer chain in the polymerized sample, the broadening FWHM due to the diffusion of *cis*-azobenzene monomers was prevented. The FWHM of the polymerized sample could retain its value near to the FWHM of UV light.

3.3.2. The capability of photo-controlled transportation

The previous study proposed that the change in the concentration of manipulated impurities was proportional to the change in the scalar order parameter, which varied linearly with $|\Delta n-\Delta n_0|/\Delta n_0$[12]. Therefore, we plotted the $|\Delta n-\Delta n_0|/\Delta n_0$ of the non-polymerized and

polymerized samples (calculated from Fig. **3.8a** and **3.8b**, respectively) with various UV exposure time, as shown in **Fig. 3.10**, to evaluate the capability of photo-controlled transportation. The $|\Delta n-\Delta n_0|/\Delta n_0$ of the polymerized sample significantly depended on the UV exposure time, while that of the non-polymerized sample only slightly increased to 0.013 after 80 s UV irradiation.

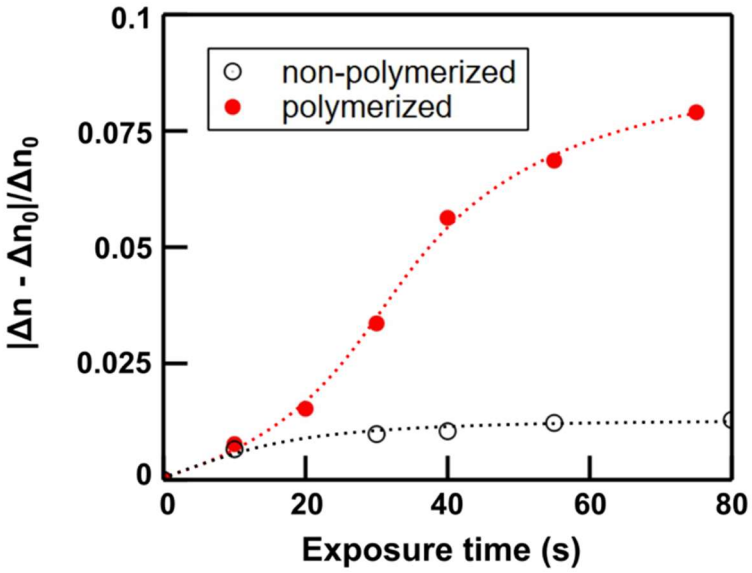

Fig. 3.10 $|\Delta n-\Delta n_0|/\Delta n_0$ to the various UV exposure time.

We explain the results of **Fig. 3.10** based on the mechanism proposed in subsection 3.3.1. In the non-polymerized sample, the scalar order parameter decreased over a wide range due to the diffusion of *cis*-azobenzene, as shown in **Fig. 3.9**. Therefore, the diffusion of *cis*-azobenzene caused a low concentration of *cis*-azobenzene in the illuminated area, leading to small values of $|\Delta n-\Delta n_0|/\Delta n_0$. In contrast, the polymerized samples had large values of $|\Delta n-\Delta n_0|/\Delta n_0$ since the cis-isomers were immobilized within the UV irradiated area. The polymerized sample which had the larger values of $|\Delta n-\Delta n_0|/\Delta n_0$ was expected to provide

high efficiencies of the photo-controlling[12]. According to the above discussions, the polymerized samples provided the high spatial resolution of the photo-induced variation of S through the immobilization of azobenzene.

3.4. The relation between the total monomer concentration and the photo-induced spatial variation of Δn

Since the polymer concentration could greatly influence the electro-optic properties of PSLCs[70,71,74], the relation between $|\Delta n-\Delta n_0|/\Delta n_0$ and the total monomer concentration was also investigated. The total monomer concentration was defined as the sum of the concentration of Azo-M and RM257. The samples with the total monomer concentration varied from 2 wt% to 8 wt% were prepared with a fixed ratio of Azo-M to RM257 = 1:1 and all the mass ratios of the monomers and the photo-initiator were fixed at 10:1. The $|\Delta n-\Delta n_0|/\Delta n_0$ values of these samples were measured under variant UV dose (**Fig. 3.11**). Each concentration had the $|\Delta n-\Delta n_0|/\Delta n_0$ values proportional to the UV dose. Under the same UV dose, $|\Delta n-\Delta n_0|/\Delta n_0$ increased with adding total monomer concentration until the highest value at 6 wt%. As the total monomer concentration increased to 8 wt%, the value of $|\Delta n-\Delta n_0|/\Delta n_0$ became smaller than that of 6 wt%.

The total-monomer-concentration-dependent increase of $|\Delta n-\Delta n_0|/\Delta n_0$ was attributed to the concentration of *cis* isomer in the irradiated area. The higher total monomer concentration suggested that the more azobenzene groups existed in the irradiated area. Thus, the sample with a higher total monomer concentration had a larger $|\Delta n-\Delta n_0|/\Delta n_0$ because more *cis*-azobenzene groups were generated under a given UV dose. On the other hand, the decrease of $|\Delta n-\Delta n_0|/\Delta n_0$ from 6 wt% to 8 wt% might be associated with the LC molecules trapped inside the dense polymer network, similar to the previously reported constrain of LC in PSLCs[70,71,74]. However, the real dynamics in the *cis* isomer and the constrained LC remained unclear without sufficient evidence. More studies should be devoted to a considerate explanation for such decrease in the future.

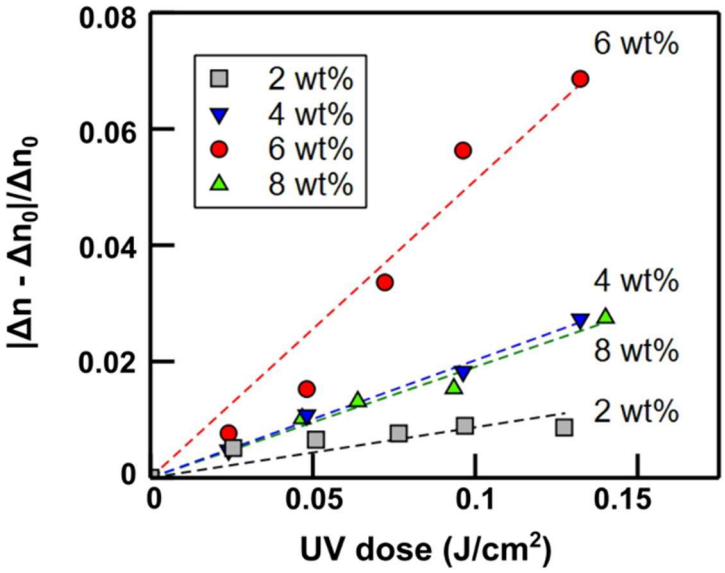

Fig. 3.11 The $|\Delta n-\Delta n_0|/\Delta n_0$ values under variant UV dose with the total monomer concentration varied from 2 wt% to 8 wt%.

We also analyzed the FWHM for total monomer concentration = 2 wt% ~ 8 wt% under various UV doses (**Fig. 3.12**). With the increase of UV dose, the FWHM of 2 wt% increased from 17 μm to 27 μm, while the FWHM of 4 wt%, 6 wt%, 8 wt% were constrained. The increasing tendency of FWHM found in 2 wt% was similar to the non-polymerized sample (**Fig. 3.9**). The results suggested that the diffusion of cis-azobenzene containing polymer was still a dominant parameter of the photo-induced spatial variation of Δn in 2 wt%. When the total monomer concentration increased to ≧ 4 wt%, the diffusion of the polymer could be ignored possibly due to the sufficient molecular weight of the polymer. The samples for 4 wt% to 8 wt% could maintain a low value of FWHM.

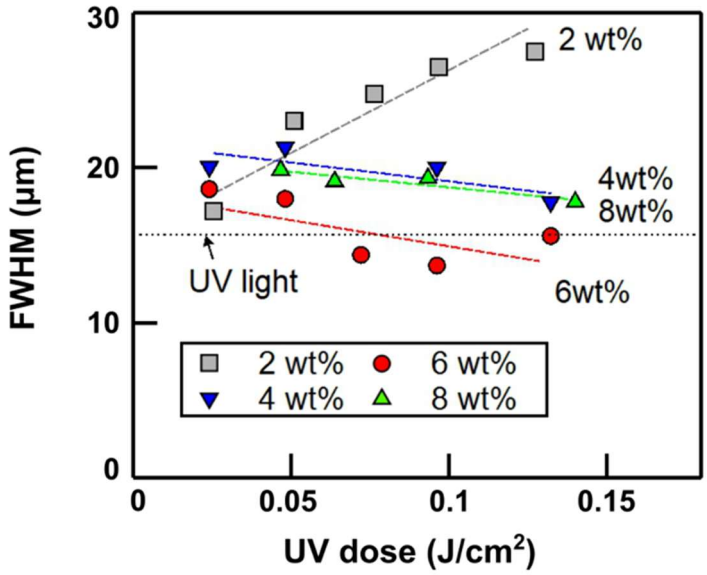

Fig. 3.12 The FWHM as a function of UV dose measured with variant total monomer concentration. The dotted line is the FWHM of UV light.

3.5. **Summary**

We have demonstrated an azobenzene-doped LC material for modulating the scalar order parameter with high spatial resolution. The comparison of the non-polymerized sample and the polymerized sample showed that the deterioration of resolution resulted from the diffusion of azobenzene molecules was largely reduced by the polymerization. This strategy for depressing the diffusion of azobenzene could be achieved when having the total monomer concentration not less than 4 wt%. The best resolution was obtained at the total monomer concentration of 6 wt%.

Chapter 4 General conclusions

Improving the spatial resolution of the light-modulated scalar order parameter helps high precision manipulating nanometer-sized impurities in the liquid crystals. In this thesis, we proposed the immobilization of azobenzene through polymerization to improve the poor resolution of the molecular manipulator. The liquid crystal gels, which consisted of the nematic LC molecules and the azobenzene-containing copolymer, were constructed after the polymerization of azobenzene monomers within the nematic phase. Their photo-response under UV light was investigated by measuring the photo-induced spatial variation of birefringence (Δn). We summarized the findings of this thesis in the following paragraphs.

In **Chapter 2**, we described the anomalous increase of Δn that was newly observed in the LC gels. To clarify the mechanism of the increase of Δn, the photo-induced change of Δn and the morphology of the copolymer microstructure were investigated with the variant composition of the LC gels. The shape of the copolymer microstructure, which had a finite anchoring strength on its surface, influenced the orientation of LC and resulted in a lower Δn of the LC gels. We proposed that the increase of Δn was attributed to the photo-induced change of the surface anchoring. The magnetic-field-induced orientation in this system was studied to clarify that the photo-induced cis-azobenzene on the copolymer microstructure decreased the anchoring strength. We concluded that the distortion in the orientation of LC due to the copolymer microstructure was weakened through the *trans*-to-*cis* isomerization of azobenzene. The orientation of LC recovered to the original uniform distribution, and thus showed the increase of Δn. The present strategy for modulating the optical property of LCs could offer a possibility to design advance functional LC materials through the photo-responsive microstructure.

In **Chapter 3**, we demonstrated the high spatial resolution of the light-modulated scalar order parameter (*S*) in an azobenzene-doped liquid crystal. Immobilization of azobenzene through polymerization was proposed to prevent the diffusion of azobenzene in the nematic phase. The photo-induced variation of birefringence of the non-polymerized and the polymerized samples was investigated to quantitatively evaluate the improved spatial resolution. The resolution of the non-polymerized sample decayed with time, while the polymerized sample remained the feature close to that of the stimulating light. The high spatial resolution achieved by this simple strategy addresses the needs for precisely-organizing nanometer-sized impurities in the liquid crystal. We believe that this LC system could serve as a template for manipulating functional nm-sized materials, *e.g.* noble metal nanoparticles and conducting polymer, leading to new fabrication of tunable photonic structure or metamaterial in the future.

Acknowledgment

First, I would like to thank my supervisor Prof. Dr. Jun Yamamoto for giving me a chance to study liquid crystal in Soft Matter Physics Group, Kyoto University. When I was preparing the documents to apply scholarship of Japan-Taiwan Exchange Association, Prof. Yamamoto kindly taught me how to prepare the research proposal, even we didn't meet before. Thank you for trusting the foreign student. During the 3.5 years (0.5 years for Research Student, 3 years for PhD Course) in Soft Matter Physics Group, Prof. Yamamoto gave me great supports, also provided me full freedom for doing my research. Especially, I want to appreciate his guidance in writing scientific papers.

I would like to thank Prof. Yoichi Takanishi for teaching me the techniques of preparing LC cells. I also want to thank his kind concerning for our health during this special period of COVID-19. I would like to appreciate Dr. Yoko Ishii. She not only gave me scientific suggestions on my experiment results and discussed it with me but also introduced me to join the world of *sado*. She was always very kind to me, and also introduced many delicious foods in Kyoto City to me. I really appreciate that she always kindly answer my questions about the culture of Japan. She even gave me kimono and taught me how to wear it to join the tea ceremony. Here I want to express my thankfulness again to Dr. Yoko Ishii. I love Kyoto more and more because of her.

In 2017, I came to Kyoto University and started the new life of the research student. At that time, Dr. Waki Sakatsuji was sitting next to me. She was very kind to me when my Japanese was still very poor. She was always concerned about me and cared about my life in Japan. I would like to thank her again here. She really helped a lot during my first-coming period. I also want to thank Chikakiyo-san. It is very nice to meet you. We always had

delicious meals together after the seminar. I also thank other of my lab members who are not specifically mentioned here. Thank you all for hearing my presentation and monthly report.

I want to thank my friends in Taiwan who support me a lot. They are Chang Chia-Ning, Liao Ya-Hsuan, and Yu Chia-Pei. I especially thank Chang Chia-Ning. She came here to visit me 3 times.

I would like to give my special thanks to my mom, my dad, and my younger brother. Thank you for always supporting me and encouraging me during my study in Japan. I wish my brother Chien Wei-Chen can smoothly get his PhD degree. Thank you for taking mom and dad to Japan to visit me. I was very happy to have a drive with my family in Japan.

Finally, I want to thank Mr. Wu Cheng-Tse. Thank you for coming here with me to pursue PhD together. I'm very glad to have you living with me in Japan.

致謝

最後我想要在交博士論文的前夕，用我的母語感謝我的家人。

謝謝我的家人:爸爸錢紫貴，媽媽余雪平，弟弟錢偉臣。我想你們，謝謝每次來找我玩還有為我加油打氣。從 2017 到 2019 我們一起住了京都町家，賞紅葉，還有開車兜風去了三方五湖，琵琶湖，和淡路島泡溫泉。媽媽還每年寄芒果給我，讓我在日本思鄉的生活還能嘗到台灣的水果。這些都是我留學生涯美好的回憶。然後，我還要謝謝吳承澤，陪我度過 2017 剛來日本胼手胝足還有壓力爆棚的生活，然後一直一起努力到現在 2020 年。很開心我們可以一起拿到台日交流協會獎學金，在京都冒險並完成學業。

在這裡我把我的博論獻給我最愛的家人們。

2020.8.31 錢巧縈 寫於京都修学院

References

[1] I.W. Stewart, The static and dynamic continuum theory of liquid crystals: a mathematical introduction, CRC Press, 2004.

[2] P. Poulin, H. Stark, T.C. Lubensky, D.A. Weitz, Novel colloidal interactions in anisotropic fluids, Science 275 (1997) 1770–1773. https://doi.org/10.1126/science.275.5307.1770.

[3] R.W. Ruhwandl, E.M. Terentjev, Long-range forces and aggregation of colloid particles in a nematic liquid crystal, Phys. Rev. E. 55 (1997) 2958–2961. https://doi.org/10.1103/PhysRevE.55.2958.

[4] J. Yamamoto, H. Tanaka, Transparent nematic phase in a liquid-crystal-based microemulsion, Nature. 409 (2001) 321–325. https://doi.org/10.1038/35053035.

[5] M. Yada, J. Yamamoto, H. Yokoyama, Direct observation of anisotropic interparticle forces in nematic colloids with optical tweezers, Phys. Rev. Lett. 92 (2004) 185501. https://doi.org/10.1103/PhysRevLett.92.185501.

[6] I.I. Smalyukh, O.D. Lavrentovich, A.N. Kuzmin, A. V. Kachynski, P.N. Prasad, Elasticity-mediated self-organization and colloidal interactions of solid spheres with tangential anchoring in a nematic liquid crystal, Phys. Rev. Lett. 95 (2005) 157801. https://doi.org/10.1103/PhysRevLett.95.157801.

[7] H. Stark, Physics of colloidal dispersions in nematic liquid crystals, Phys. Rep. 351 (2001) 387–474.

[8] O.D. Lavrentovich, Transport of particles in liquid crystals, Soft Matter. 10 (2014) 1264–1283. https://doi.org/10.1039/C3SM51628H.

[9] C. Blanc, D. Coursault, E. Lacaze, Ordering nano-and microparticles assemblies with liquid crystals, Liq. Cryst. Rev. 1 (2013) 83–109. https://doi.org/10.1080/21680396.2013.818515.

[10] A. Nych, U. Ognysta, M. Škarabot, M. Ravnik, S. Žumer, I. Muševič, Assembly and control of 3D nematic dipolar colloidal crystals, Nat. Commun. 4 (2013). https://doi.org/10.1038/ncomms2486.

[11] I. Muševič, Integrated and topological liquid crystal photonics, Liq. Cryst. 41 (2014) 418–429. https://doi.org/10.1080/02678292.2013.837516.

[12] S. Samitsu, Y. Takanishi, J. Yamamoto, Molecular manipulator driven by spatial variation of liquid-crystalline order, Nat. Mater. 9 (2010) 816–820. https://doi.org/10.1038/nmat2853.

[13] M. Hara, H. Takezoe, A. Fukuda, Forced rayleigh scattering in ncb's (N = 5-9) with methyl red and binary mass diffusion constants, Jpn. J. Appl. Phys. 25 (1986) 1756–1761. https://doi.org/10.1143/JJAP.25.1756.

[14] R.A. Sabet, H. Khoshsima, Real-time holographic investigation of azo dye diffusion in a nematic liquid crystal host, Dye. Pigment. 87 (2010) 95–99. https://doi.org/10.1016/j.dyepig.2010.02.009.

[15] M. Pumpa, F. Cichos, Slow single-molecule diffusion in liquid crystals, J. Phys. Chem. B. 116 (2012) 14487–14493. https://doi.org/10.1021/jp307403w.

[16] M. Kleman, O.D. Lavrentovich, Soft Matter Physics: An Introduction, Springer, 2003. https://doi.org/10.1007/b97416.

[17] P.-G. De Gennes, J. Prost, The physics of liquid crystals, 2nd ed., Oxford university press, 1993.

[18] J.W. Goodby, P.J. Collings, T. Kato, H. Gleeson, C. Tschierske, V. Vill, P. Raynes, Handbook of Liquid Crystals, 8 Volume Set, John Wiley & Sons, 2014.

[19] T.C. Lubensky, D. Pettey, N. Currier, H. Stark, Topological defects and interactions in nematic emulsions, Phys. Rev. E. 57 (1998) 610–625. https://doi.org/10.1103/PhysRevE.57.610.

[20] B. Jérôme, Surface effects and anchoring in liquid crystals, Reports Prog. Phys. 54 (1991) 391–451. https://doi.org/10.1088/0034-4885/54/3/002.

[21] I. Muševič, Liquid crystal colloids, Springer, 2017.

[22] M. ŠKarabot, I. Muševič, Direct observation of interaction of nanoparticles in a nematic liquid crystal, Soft Matter. 6 (2010) 5476–5481. https://doi.org/10.1039/c0sm00437e.

[23] M. Škarabot, M. Ravnik, S. Žumer, U. Tkalec, I. Poberaj, D. Babič, N. Osterman, I. Muševič, Interactions of quadrupolar nematic colloids, Phys. Rev. E. 77 (2008) 1–8. https://doi.org/10.1103/PhysRevE.77.031705.

[24] J. ichi Fukuda, H. Stark, M. Yoneya, H. Yokoyama, Interaction between two spherical particles in a nematic liquid crystal, Phys. Rev. E. 69 (2004) 10. https://doi.org/10.1103/PhysRevE.69.041706.

[25] I. Musevič, M. Skarabot, Self-assembly of nematic colloids, Soft Matter. 4 (2008) 195. https://doi.org/10.1039/b714250a.

[26] I. Muševič, M. Škarabot, U. Tkalec, M. Ravnik, S. Žumer, Two-dimensional nematic colloidal crystals self-assembled by topological defects, Science 313 (2006) 954–958. https://doi.org/10.1126/science.1129660.

[27] U. Ognysta, A. Nych, V. Nazarenko, I. Muševič, M. Škarabot, M. Ravnik, S. Žumer, I. Poberaj, D. Babič, 2D interactions and binary crystals of dipolar and quadrupolar nematic colloids, Phys. Rev. Lett. 100 (2008) 7–10. https://doi.org/10.1103/PhysRevLett.100.217803.

[28] H.K. Bisoyi, Q. Li, Light-Driven Liquid Crystalline Materials: From Photo-Induced Phase Transitions and Property Modulations to Applications, Chem. Rev. 116 (2016) 15089–15166. https://doi.org/10.1021/acs.chemrev.6b00415.

[29] Y. Zhao, T. Ikeda, Smart Light-Responsive Materials: Azobenzene-Containing Polymers and Liquid Crystals, John Wiley & Sons, 2009. https://doi.org/10.1002/9780470439098.

[30] J.H. Sung, S. Hirano, O. Tsutsumi, A. Kanazawa, T. Shiono, T. Ikeda, Dynamics of photochemical phase transition of guest/host liquid crystals with an azobenzene derivative as a photoresponsive chromophore, Chem. Mater. 14 (2002) 385–391. https://doi.org/10.1021/cm010729m.

[31] A. Matsuyama, T. Kato, Phase separations and orientational ordering of polymers in liquid crystal solvents, Phys. Rev. E. 59 (1999) 763–770. https://doi.org/10.1103/PhysRevE.59.763.

[32] M. Škarabot, Ž. Lokar, I. Muševič, Transport of particles by a thermally induced gradient of the order parameter in nematic liquid crystals, Phys. Rev. E. 87 (2013) 1–6. https://doi.org/10.1103/PhysRevE.87.062501.

[33] S.A. Tatarkova, D.R. Burnham, A.K. Kirby, G.D. Love, E.M. Terentjev, Colloidal interactions and transport in nematic liquid crystals, Phys. Rev. Lett. 98 (2007) 1–4. https://doi.org/10.1103/PhysRevLett.98.157801.

[34] G.M. Koenig Jr., J.J. De Pablo, N.L. Abbott, Characterization of the reversible interaction of pairs of nanoparticles dispersed in nematic liquid crystals, Langmuir. 25 (2009) 13318–13321. https://doi.org/10.1021/la903464t.

[35] A. V. Ryzhkova, I. Muševič, Particle size effects on nanocolloidal interactions in nematic liquid crystals, Phys. Rev. E. 87 (2013) 1–12. https://doi.org/10.1103/PhysRevE.87.032501.

[36] B. Senyuk, J.S. Evans, P.J. Ackerman, T. Lee, P. Manna, L. Vigderman, E.R. Zubarev, J. Van De Lagemaat, I.I. Smalyukh, Shape-dependent oriented trapping and scaffolding of plasmonic nanoparticles by topological defects for self-assembly of colloidal dimers in liquid crystals, Nano Lett. 12 (2012) 955–963. https://doi.org/10.1021/nl204030t.

[37] D. Voloschenko, O.P. Pishnyak, S. V. Shiyanovskii, O.D. Lavrentovich, Effect of director distortions on morphologies of phase separation in liquid crystals, Phys. Rev. E. 65 (2002). https://doi.org/10.1103/PhysRevE.65.060701.

[38] H. Yoshida, Y. Tanaka, K. Kawamoto, H. Kubo, T. Tsuda, A. Fujii, S. Kuwabata, H. Kikuchi, M. Ozaki, Nanoparticle-stabilized cholesteric blue phases, Appl. Phys. Express. 2 (2009). https://doi.org/10.1143/APEX.2.121501.

[39] E. Karatairi, B. Rožič, Z. Kutnjak, V. Tzitzios, G. Nounesis, G. Cordoyiannis, J. Thoen, C. Glorieux, S. Kralj, Nanoparticle-induced widening of the temperature range of liquid-crystalline blue phases, Phys. Rev. E. 81 (2010) 1–5. https://doi.org/10.1103/PhysRevE.81.041703.

[40] T. Ikeda, Photomodulation of liquid crystal orientations for photonic applications, J. Mater. Chem. 13 (2003) 2037–2057. https://doi.org/10.1039/b306216n.

[41] K.G. Yager, C.J. Barrett, Novel photo-switching using azobenzene functional materials, J. Photochem. Photobiol. A Chem. 182 (2006) 250–261. https://doi.org/10.1016/j.jphotochem.2006.04.021.

[42] H.M.D. Bandara, S.C. Burdette, Photoisomerization in different classes of azobenzene, Chem. Soc. Rev. 41 (2012) 1809–1825. https://doi.org/10.1039/c1cs15179g.

[43] E.M.M. Tan, S. Amirjalayer, S. Smolarek, A. Vdovin, F. Zerbetto, W.J. Buma, Fast photodynamics of azobenzene probed by scanning excited-state potential energy

surfaces using slow spectroscopy, Nat. Commun. 6 (2015). https://doi.org/10.1038/ncomms6860.

[44] M. Quick, A.L. Dobryakov, M. Gerecke, C. Richter, F. Berndt, I.N. Ioffe, A.A. Granovsky, R. Mahrwald, N.P. Ernsting, S.A. Kovalenko, Photoisomerization dynamics and pathways of trans- and cis- azobenzene in solution from broadband femtosecond spectroscopies and calculations, J. Phys. Chem. B. 118 (2014) 8756–8771. https://doi.org/10.1021/jp504999f.

[45] Y. Yu, T. Ikeda, Alignment modulation of azobenzene-containing liquid crystal systems by photochemical reactions, J. Photochem. Photobiol. C Photochem. Rev. 5 (2004) 247–265. https://doi.org/10.1016/j.jphotochemrev.2004.10.004.

[46] C. Ruslim, I. Kunihiro, Z-Isomers of Azobenzenes Highly Compatible with Liquid Crystals, Chem. Lett. 27 (1998) 789–790.

[47] T. Ikeda, T. Miyamoto, S. Kurihara, S. Tazuke, Effect of Structure of Photoresponsive Molecules on Photochemical Phase Transition of Liquid Crystals III. Photochemical Phase Transition Behaviors of Photochromic Azobenzene Guest/Ester Host Mixtures, Mol. Cryst. Liq. Cryst. Inc. Nonlinear Opt. 188 (1990) 207–222. https://doi.org/10.1080/00268949008047818.

[48] T. Ikeda, T. Miyamoto, S. Kurihara, S. Tazuke, Effect of Structure of Photoresponsive Molecules on Photochemical Phase Transition of Liquid Crystals IV. Photochemical Phase Transition Behaviors of Photochromic Azobenzene Guest/ Polymer Liquid Crystal Host Mixtures, Mol. Cryst. Liq. Cryst. Inc. Nonlinear Opt. 188 (1990) 223–233. https://doi.org/10.1080/00268949008047819.

[49] S. Kurihara, T. Ikeda, S. Tazuke, Photochemically Induced Isothermal Phase Transition in Liquid Crystals. Effect of Interaction of Photoresponsive Molecules with

Matrix Mesogens, Mol. Cryst. Liq. Cryst. Inc. Nonlinear Opt. 178 (1990) 117–132. https://doi.org/10.1080/00268949008042713.

[50] T. Ikeda, S. Horiuchi, D.B. Karanjit, S. Kurihara, S. Tazuke, Photochemical Image Storage in Polymer Liquid Crystals, Chem. Lett. 17 (1988) 1679–1682.

[51] T. Ikeda, S. Horiuchi, D.B. Karanjit, S. Kurihara, S. Tazuke, Photochemically Induced Isothermal Phase Transition in Polymer Liquid Crystals with Mesogenic Phenyl Benzoate Side Chains. 1. Calorimetric Studies and Order Parameters, Macromolecules. 23 (1990) 36–42. https://doi.org/10.1021/ma00203a008.

[52] T. Ikeda, S. Horiuchi, D.B. Karanjit, S. Kurihara, S. Tazuke, Photochemically Induced Isothermal Phase Transition in Polymer Liquid Crystals with Mesogenic Phenyl Benzoate Side Chains. 2. Photochemically Induced Isothermal Phase Transition Behaviors, Macromolecules. 23 (1990) 42–48. https://doi.org/10.1021/ma00203a009.

[53] M. Eich, B. Reck, H. Ringsdorf, J.H. Wendorff, Reversible Digital And Holographic Optical Storafe In Polymeric Liquid Crystals (PLC), Die Makromol. Chemie, Rapid Commun. 8 (1987) 59–63. https://doi.org/10.1117/12.939643.

[54] T. Ikeda, O. Tsutsumi, Optical switching and image storage by means of azobenzene liquid-crystal films, Science 268 (1995) 1873–1875. https://doi.org/10.1126/science.268.5219.1873.

[55] K. Ichimura, Photoalignment of Liquid-Crystal Systems, Chem. Rev. 100 (2000) 1847–1873. https://doi.org/10.1021/cr980079e.

[56] M. Han, S. Morino, K. Ichimura, Factors affecting in-plane and out-of-plane photoorientation of azobenzene side chains attached to liquid crystalline polymers induced by irradiation with linearly polarized light, Macromolecules. 33 (2000) 6360–6371. https://doi.org/10.1021/ma000347m.

[57] M. Han, K. Ichimura, Tilt orientation of p-methoxyazobenzene side chains in liquid crystalline polymer films by irradiation with nonpolarized light, Macromolecules. 34 (2001) 82–89. https://doi.org/10.1021/ma0008239.

[58] A. Natansohn, P. Rochon, Photoinduced motions in azo-containing polymers, Chem. Rev. 102 (2002) 4139–4175. https://doi.org/10.1021/cr970155y.

[59] L. Corvazier, Y. Zhao, Induction of liquid crystal orientation through azobenzene-containing polymer networks, Macromolecules. 32 (1999) 3195–3200. https://doi.org/10.1021/ma9818811.

[60] K. Ichimura, Y. Suzuki, T. Seki, A. Hosoki, K. Aoki, Reversible change in alignment mode of nematic liquid crystals regulated photochemically by "command surfaces" modified with an azobenzene monolayer, Langmuir. 4 (1988) 1214–1216. https://doi.org/10.1021/la00083a030.

[61] T. Seki, M. Sakuragi, Y. Kawanishi, Y. Suzuki, T. Tamaki, R. ichi Fukuda, K. Ichimura, "Command Surfaces" of Langmuir-Blodgett Films. Photoregulations of Liquid Crystal Alignment by Molecularly Tailored Surface Azobenzene Layers, Langmuir. 9 (1993) 211–218. https://doi.org/10.1021/la00025a041.

[62] W.M. Gibbons, P.J. Shannon, S.-T. Sun, B.J. Swetlin, Surface-mediated alignment of nematic liquid crystals with polarized laser light, Nature. 351 (1991) 49–50. https://doi.org/10.1080/02678299208029130.

[63] I. Dierking, Polymer network-stabilized liquid crystals, Adv. Mater. 12 (2000) 167–181. https://doi.org/10.1002/(SICI)1521-4095(200002)12:3<167::AID-ADMA167>3.0.CO;2-I.

[64] I. Dierking, Recent developments in polymer stabilised liquid crystals, Polym. Chem. 1 (2010) 1153–1159. https://doi.org/10.1039/c0py00087f.

[65] I. Dierking, A review of polymer-stabilized ferroelectric liquid crystals, Materials (Basel). 7 (2014) 3568–3587. https://doi.org/10.3390/ma7053568.

[66] G.A. Held, L.L. Kosbar, I. Dierking, A.C. Lowe, G. Grinstein, V. Lee, R.D. Miller, Confocal microscopy study of texture transitions in a polymer stabilized cholesteric liquid crystal, Phys. Rev. Lett. 79 (1997) 3443–3446. https://doi.org/10.1103/PhysRevLett.79.3443.

[67] I. Dierking, L.L. Kosbar, A. Afzali-Ardakani, A.C. Lowe, G.A. Held, Network morphology of polymer stabilized liquid crystals, Appiled Phys. Lett. 71 (1997) 2454–2456.

[68] C. V Rajaram, S.D. Hudson, L.C. Chien, Morphology of diacrylate copolymer networks, Polymer (Guildf). 39 (1998) 5315–5319.

[69] C. V. Rajaram, S.D. Hudson, L.C. Chien, Effect of Polymerization Temperature on the Morphology and Electrooptic Properties of Polymer-Stabilized Liquid Crystals, Chem. Mater. 8 (1996) 2451–2460. https://doi.org/10.1021/cm9505207.

[70] R. Ma, D. Yang, Freedericksz transition in polymer-stabilized nematic liquid crystals, Phys. Rev. E. 61 (2000) 1567–73. https://doi.org/10.1103/physreve.61.1567.

[71] Y.K. Fung, A. Borstnik, S. Zumer, D.K. Yang, J.W. Doane, Pretransitional nematic ordering in liquid crystals with dispersed polymer networks, Phys. Rev. E. 55 (1997) 1637–1645. https://doi.org/10.1103/PhysRevE.55.1637.

[72] R.E. Kraig, P.L. Taylor, R. Ma, D.K. Yang, Nematic order in polymer-stabilized liquid crystals, Phys. Rev. E. 58 (1998) 4594–4597. https://doi.org/10.1103/PhysRevE.58.4594.

[73] P.A. Kossyrev, J. Qi, N. V. Priezjev, R.A. Pelcovits, G.P. Crawford, Virtual surfaces, director domains, and the Fréedericksz transition in polymer-stabilized nematic liquid crystals, Appl. Phys. Lett. 81 (2002) 2986–2988. https://doi.org/10.1063/1.1515136.

[74] D.K. Yang, Y. Cui, H. Nemati, X. Zhou, A. Moheghi, Modeling aligning effect of polymer network in polymer stabilized nematic liquid crystals, J. Appl. Phys. 114 (2013) 243515. https://doi.org/10.1063/1.4856295.

[75] H. Tajalli, A.G. Gilani, M.S. Zakerhamidi, P. Tajalli, The photophysical properties of Nile red and Nile blue in ordered anisotropic media, Dye. Pigment. 78 (2008) 15–24. https://doi.org/10.1016/j.dyepig.2007.10.002.

[76] T. Araki, M. Buscaglia, T. Bellini, H. Tanaka, Memory and topological frustration in nematic liquid crystals confined in porous materials, Nat. Mater. 10 (2011) 303–309. https://doi.org/10.1038/nmat2982.

[77] T. Yamamoto, Y. Tabe, H. Yokoyama, Photochemical transformation of topological defects formed around colloidal droplets dispersed in azobenzene-containing liquid crystals, Colloids Surfaces A Physicochem. Eng. Asp. 334 (2009) 155–159. https://doi.org/10.1016/j.colsurfa.2008.10.010.